Micromechanical schemes for Stokes to Darcy homogenization of permeability based on generalized Brinkman inhomogeneity problems

François Bignonnet

Micromechanical schemes for Stokes to Darcy homogenization of permeability based on generalized Brinkman inhomogeneity problems

François Bignonnet

GeM, Research Institute of Civil Engineering and Mechanics, UMR CNRS 6183, Université de Nantes, France

Abstract

Mean field homogenization schemes are formulated for the Stokes to Darcy upscaling of the permeability on the basis of generalized inhomogeneity problems in which flow is described by Brinkman equations. The average velocity and drag force concentrations for flow in a potentially composite inclusion are characterized in terms of a permeability contribution tensor and an equivalent permeability, which allow for the direct transposition to Stokes to Darcy upscaling of most homogenization schemes available in elasticity (self-consistent, differential, Mori-Tanaka, Maxwell, ...). The unified framework extends existing effective medium and cell model permeability estimates. Its flexibility is illustrated on a panel of microstructures of porous media: granular or fibrous materials, materials with spanning cylindrical or crack-like pores, double porosity materials with disconnected or connected meso-porosity and compared with existing or newly produced full field simulation results.

Keywords: Permeability, Homogenization, Porous Media, Stokes flow, Brinkman equation, Effective medium

1. Introduction

Continuum micromechanics [1–5] is a framework to upscale material properties from microstructure information. The area of homogenization of elastic or conductive properties of disordered heterogeneous materials has developed intensively since the work of Eshelby [6, 7] on the concentration of elastic fields in an isolated ellipsoidal inhomogeneity surrounded by an unbounded reference material. The inhomogeneity problem of Eshelby has laid the foundations of a series of *homogenization schemes* to *estimate* the effective stiffness or conduction of heterogeneous media from targeted and limited microstructure information such as the stiffness or conduction of the constituents, their volume fraction, the approximate shape of the heterogeneities. Information on the interactions of the heterogeneities is implicitly accounted for by the choice of an appropriate homogenization scheme, such as: the dilute scheme, the Mori-Tanaka scheme [8, 9], the differential scheme [10–15], Maxwell's estimate [16, 17], the self-consistent scheme or effective medium approximation [18–22].

A related yet different problem lies in the upscaling of the permeability of a porous material, where flow is described by Darcy equations at the macroscopic scale and by Stokes equations at the microscopic scale, within the pore space. The emergence of Darcy equations from Stokes equations is well documented and justified by multi-scale asymptotic series expansions or averaging techniques [23–27]. However, the *estimation* of the effective permeability of a porous medium from targeted microstructure information and homogenization schemes at the scale of the pores and solid particles has undergone a distinct and perhaps narrower development than in elasticity or conduction.

The present contribution investigates the formulation of homogenization schemes for Stokes to Darcy upscaling of disordered porous media, directly inspired from their continuum micromechanics counterparts

*Corresponding author. Tel.: +33-2-40-17-81-89. Address: 58 rue Michel Ange, 44600 Saint-Nazaire, France

available for elasticity or conduction. Homogenization schemes are indeed believed useful alternatives to full field numerical simulations of flow within an explicit representative volume element of the pore space [28–31] or to pore network models [32] when computational cost is a concern or available microstructure information is limited. The derived estimates can apply to both single porosity materials, in which all pores have the same length scale, and double or multiple porosity materials, which have pores sizes spread over distinct length scales.

Most of the existing estimates for Stokes to Darcy homogenization are build from either (1) the solution to Poiseuille's flow in a cylindrical or planar pore or (2) a single composite cell problem which feature a solid, potentially porous core surrounded by a fluid envelope. The effective permeability is derived from the relation between the applied velocity and the pressure drop or resultant drag force.

Models based on Poiseuille's flow have been widely used since the seminal work of Carman [33]. Poiseuille's flow has also been used in Darcy to Darcy homogenization schemes by replacing pores with a cylindrical or planar shape by a fictitious porous region with an equivalent permeability to account e.g. for cracks [34–36] or interface effects [37, 38]. This strategy has been extended to crack networks using discrete versions of the homogenization schemes to better account for percolation effects [39]. However, these methods cannot account for other pore shapes.

Models based on composite cells deliver simple and efficient estimates to the permeability of granular or fibrous media. Two class of estimates have been formulated. In the first one, to which we will refer as *cell models*, the boundary conditions are applied directly at the surface of the composite cell. Various types of boundary conditions have been investigated: uniform velocity prescribed on both normal and tangential directions [40], or on the normal direction only together with either zero shear stress [41–45] or zero vorticity [46]. Most cell models consider spherical or cylindrical geometries, but approximate formulas for their extensions to spheroidal particles have been derived [47]. The solid core can be either impermeable [41, 42, 45–47], porous [43, 48–50] or multi-layered [51]. In the second class of estimate, called *Effective Medium Approximation* (EMA), the composite cell is embedded in an unbounded reference porous domain [52–57] with infinitely remote boundary conditions, akin to Eshelby inhomogeneity problem. The permeability of the reference medium is determined from a self-consistency argument: the drag force within the composite cell must match the one that there would be if the composite cell where replaced by the reference medium. While early studies assumed continuity of both the velocity and stress at the fluid – porous medium interface, more recent contributions [50, 51, 57] have accounted for a "jump momentum" discontinuity condition of the shearing stress at a fluid – porous medium interface deduced by Ochoa-Tapia and Whitaker [58, 59] from an averaging procedure of Navier-Stokes equations.

In these estimates, Brinkman's equations [60] are used instead of Darcy's equations in the reference medium (and in the porous parts of the core, if any) in order to retain information regarding the shear stress at the fluid envelope – porous medium interface. The Brinkman corrective term to Stokes equations has been shown to arise from multiscale asymptotic series expansion with poor separation of scales for flow in non-homogeneous porous media [61, 62]. Brinkman [60] introduced it to derive an early version of EMA (or swarm model) from the problem of an isolated spherical solid particle embedded in an infinite porous medium in which flow is described by Brinkman's equations. Heuristically, Brinkman's equations allow to capture both the fluid shearing stress in the near field and the average drag force contribution of other particles in the far field, within a continuous approach. A key asset of Brinkman's early EMA is its ability to efficiently retrieve the correct leading term in the drag force increment due to multiple sphere interactions at low solid concentration, as later shown from more sophisticated developments on random multi-particle systems [63–65]. However at larger solid concentration, this estimate fails since the pore space is not explicitly accounted for in the isolated solid particle problem. Subsequent modifications with an explicit description of fluid by an envelope around the particle [52–54] partially correct the low porosity behavior, but break down the exact asymptotic behavior at the low solid concentration.

From an iterated dilute approximation similar in concept to the differential estimate used in elasticity [12–15], Wilkinson [66] suggested a differential scheme to improve on the early EMA of Brinkman [60] for the low porosity behavior. This differential scheme also relies on Brinkman's problem of a solid particle, without fluid envelope, surrounded by an unbounded porous medium described by Brinkman's equations.

This brief review of homogenization schemes for Stokes to Darcy upscaling (cell model, EMA, differ-

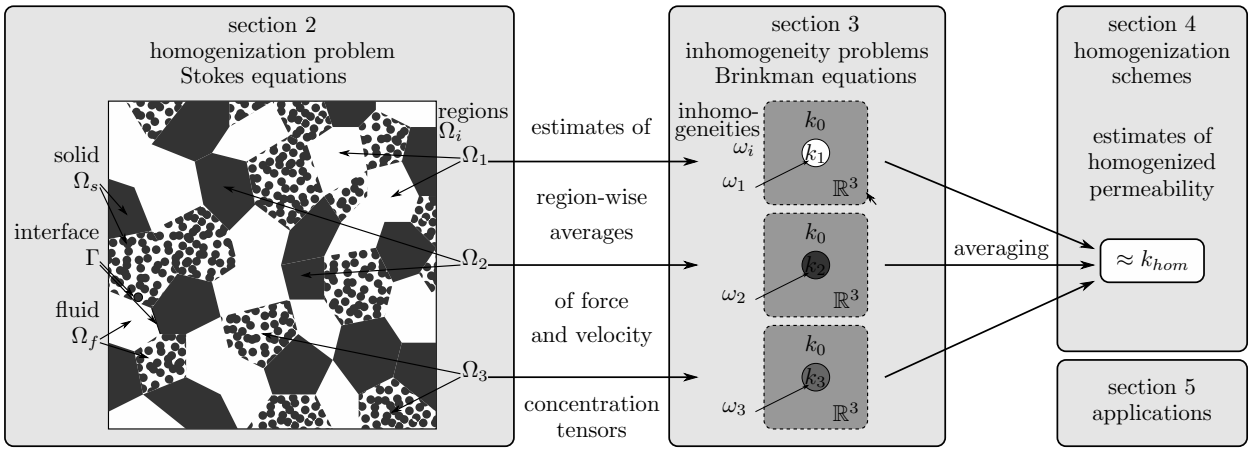

Figure 1: Graphical abstract of the article: estimates of the homogenized permeability are build via several Brinkman inhomogeneity problems, assembled by homogenization schemes, to estimate the region-wise averages of the velocity and force concentration tensors of the Stokes flow problem at the microscopic scale.

ential scheme) highlights their relative scarcity as compared to those available for elasticity or conduction upscaling. We believe that the main reason for this hindered development is the fundamental difference between these two types of problems: when homogenizing elliptic equations such as elasticity or conduction ones, an equation invariance occurs ; while the Stokes to Darcy homogenization breaks down this invariance [67]. In turn, Brinkman's equations allow working within a unified set of equations, which is beneficial for numerical simulations [67] but also for analytical homogenization techniques, as developed herein. They indeed encompass Stokes equation in the limiting case of infinite permeability, solid regions in the case of zero permeability, but also provide an approximate means to handle double or multiple porosity materials.

The article sets a theoretical framework to transpose a larger panel of homogenization schemes available in elasticity or conduction to Stokes to Darcy upscaling, including double porosity media, and is structured as follows. Section 2 provides background on well established results regarding the upscaling permeability from Stokes equations. The main original contribution is the investigation of generalized Brinkman inhomogeneity problems in section 3, including the definition of property contribution tensors and equivalent permeability of heterogeneous inclusions to prepare the adaptation of homogenization schemes. Some useful results on cell models are also presented. Several homogenization schemes classical in elasticity or conduction upscaling are then systematically transposed to Stokes to Darcy upscaling in section 4 by relying on the Brinkman inhomogeneity problems. The last original contribution in section 5 lies in the extensive comparison of the resulting homogenization schemes with a rather wide range of porous microstructures for which full field simulation results are either available or produced. Appendix A provides solutions to several inhomogeneity problems in Cartesian, cylindrical and spherical coordinates used in the article.

2. Background: homogenization of permeability from Stokes equations

The emergence of Darcy's law from upscaling Stokes flow through porous media is a well established result [23, 25–27, 45, 61, 68]. Its main aspects are recalled in this section.

2.1. Flow descriptions at the microscopic and macroscopic scales

Two scales of flow description. We consider the description of flow of an incompressible Newtonian fluid of viscosity μ through a porous medium. The order of magnitude of the velocity is denoted V_c, it is assumed sufficiently slow to neglect inertia effects. Two characteristic length scales l_c and L_c are involved. l_c represents the characteristic size of the pores while L_c represents the characteristic length of a characteristic macroscopic pressure drop δP_c. L_c is assumed of the same order of magnitude than the structure or sample scale. These scales are assumed separated, i.e. the ratio $\epsilon = l_c/L_c \ll 1$. Further, we assume that the

viscous flow which induces $\mathcal{O}(\mu V_c/l_c^2)$ terms in momentum balance at the microscopic scale is driven by the macroscopic pressure drop which is $\mathcal{O}(\delta P_c/L_c)$, hence $\mu v_c L_c/(l_c^2 p_c) = \mathcal{O}(1)$.

Macroscopic scale. At the macroscopic scale, the filtration velocity $\boldsymbol{V}$ and the pressure P are fields of the slow spatial variable $\boldsymbol{X}$. Darcy's law linearly $\boldsymbol{V}$ to the macroscopic pressure gradient $\nabla_X P$ via the permeability tensor $\boldsymbol{k}$:

$$\begin{aligned} \nabla_X \cdot \boldsymbol{V} &= 0 \\ \boldsymbol{V} &= -\frac{\boldsymbol{k}}{\mu} \cdot \nabla_X P \end{aligned} \tag{1}$$

Microscopic scale. At the microscopic scale the flow is that of an incompressible Newtonian fluid within the pore space governed by Stokes equations. Within the framework of periodic homogenization [25, 26], a homogenization problem P_{Stokes} is defined on a Representative Volume Element (RVE) Ω around a point $\boldsymbol{X}_0$ of the macroscopic scale comprising a fluid phase Ω_f, a rigid solid phase Ω_s and a solid-fluid interface Γ. The size L_Ω of the RVE must meet $L_\Omega \ll L_c$ to ensure the description by a continuum at the macroscopic scale as well as $L_\Omega \gg l_c$ to ensure the representativity of the RVE. The fluid velocity $\boldsymbol{v}$, the pressure p and the Cauchy stress tensor $\boldsymbol{\sigma}$ are fields of the fast spatial variable $\boldsymbol{x} = (\boldsymbol{X} - \boldsymbol{X}_0)/\epsilon$. Within the RVE, the macroscopic velocity $\boldsymbol{V}$ and the pressure gradient $\nabla_X P$ from (1) appears as constants for the fast spatial variable $\boldsymbol{x}$. To simplify notations in what follows, we denote $\nabla_X P$ by $\boldsymbol{F}$ which acts as a forcing term on the local flow:

$$\begin{aligned} &\nabla_x \cdot \boldsymbol{\sigma} = 0 && \text{in } \Omega_f \\ &\boldsymbol{\sigma} = -p\mathbf{1} + 2\mu\nabla_x^s \boldsymbol{v} && \text{in } \Omega_f \\ &\nabla_x \cdot \boldsymbol{v} = 0 && \text{in } \Omega_f \\ &\boldsymbol{v} = \mathbf{0} && \text{on } \Gamma \\ &\boldsymbol{v} \text{ and } p - \boldsymbol{F}\cdot\boldsymbol{x} \text{ periodic} && \text{on } \partial\Omega \end{aligned} \tag{2}$$

where $\nabla_x^s \boldsymbol{v}$ is the symmetric part of the microscopic velocity gradient and $\mathbf{1}$ the identity second order tensor. In what follows, we implicitly drop the reference to the fast space variable $\boldsymbol{x}$ in the differential operators at the microscopic scale.

By linearity of problem (2), the solution velocity field $\boldsymbol{v}$ linearly depends on $\boldsymbol{F}$ via some velocity concentration tensor field $\boldsymbol{\kappa}$ such that:

$$\forall \boldsymbol{x} \in \Omega, \quad \boldsymbol{v}(\boldsymbol{x}) = -\frac{1}{\mu}\boldsymbol{\kappa}(\boldsymbol{x}) \cdot \boldsymbol{F} \tag{3}$$

where, by extension, $\boldsymbol{v}$ is set to 0 in Ω_s.

Correspondence of the two flow descriptions. The macroscopic velocity $\boldsymbol{V}$ is related to its microscopic counterpart by the averaging rule:

$$\boldsymbol{V} = \overline{\boldsymbol{v}}^{\Omega} \quad \text{with} \quad \overline{\boldsymbol{v}}^{\Omega} = \frac{1}{|\Omega|}\int_\Omega \boldsymbol{v}\,\mathrm{d}V \tag{4}$$

where $\boldsymbol{v}$ is null in the solid phase. The combination of (3) and (4) shows that the macroscopic velocity $\boldsymbol{V}$ is linearly related to the macroscopic pressure gradient $\boldsymbol{F}$ by the permeability tensor $\boldsymbol{k}_{\text{hom}}$ of the porous medium defined as:

$$\boldsymbol{k}_{\text{hom}} = \overline{\boldsymbol{\kappa}}^{\Omega}, \tag{5}$$

to be used in (1) at the macroscopic scale. From an equivalent energy definition of $\boldsymbol{k}_{\text{hom}}$, the homogenized permeability is shown symmetric and definite positive [2].

Decomposition of the volume average over regions. A common practice in continuum micromechanics is to decompose the RVE Ω in several phases or regions $(\Omega_i)_{i=1,\dots,n}$ which form a partition of Ω (see e.g. fig. 1). Each region gathers parts of the RVE which have the same characteristics, for example all pores or solid grains of a given size, shape and orientation, or regions within which the microstructure can be described by a homogeneous random process. The volume fraction of each region Ω_i is denoted $\varphi_i = |\Omega_i|/|\Omega|$. The volume average of a field, say $\boldsymbol{\kappa}$, over the RVE then decomposes as:

$$\overline{\boldsymbol{\kappa}}^{\Omega} = \sum_{i=1}^{n} \varphi_i \overline{\boldsymbol{\kappa}}^{i} \quad \text{with} \quad \overline{\boldsymbol{\kappa}}^{i} = \frac{1}{|\Omega_i|} \int_{\Omega_i} \boldsymbol{\kappa} \, \mathrm{d}V \tag{6}$$

The homogenized permeability (5) can thus be computed from the region-wise averages $\overline{\boldsymbol{\kappa}}^{i}$.

2.2. Extension to the solid phase of the microscopic flow problem

The Stokes to Darcy upscaling problem P_{Stokes} (2) can be extended to the solid phase by considering the whole RVE Ω filled with a homogeneous Newtonian fluid of uniform viscosity μ, provided the solid phase and the no-slip condition are indirectly accounted for by an appropriate choice of a body force field $\boldsymbol{f}$ applied to the homogeneous fluid [69]:

$$\begin{aligned}
&\nabla \cdot \boldsymbol{\sigma} + \boldsymbol{f} = 0 && \text{in } \Omega \\
&\boldsymbol{\sigma} = -p\mathbf{1} + 2\mu \nabla^s \boldsymbol{v} && \text{in } \Omega \\
&\nabla \cdot \boldsymbol{v} = 0 && \text{in } \Omega \\
&\boldsymbol{v} = 0 && \text{in } \Omega_s \\
&\boldsymbol{v} \text{ and } p - \boldsymbol{F}\cdot\boldsymbol{x} \text{ periodic} && \text{on } \partial\Omega
\end{aligned} \tag{7}$$

The body force $\boldsymbol{f}$ must verify $\boldsymbol{f} = 0$ in Ω_f to retrieve local momentum balance in the "true" fluid domain Ω_f and $\overline{\boldsymbol{f}}^{\Omega} = \boldsymbol{F}$ to ensure the overall momentum balance of the RVE [69]. In other words, the average body force $\overline{\boldsymbol{f}}^{\Omega}$ exerted by the solid on the fluid is equal to the macroscopic pressure gradient $\boldsymbol{F}$.

Formally, the solution to problem P_{Stokes} (2) in Ω_f can be retrieved from the body force field:

$$\boldsymbol{f} = \boldsymbol{F} I_s + (\boldsymbol{\sigma}_{|f} + (\boldsymbol{F}\cdot\boldsymbol{x})\mathbf{1}) \cdot \nabla I_s \tag{8}$$

where $\boldsymbol{\sigma}_{|f}$ is the stress evaluated on the Ω_f side of Γ and I_s is the indicator function of the solid phase, equal to 1 in Ω_s and 0 in Ω_f. The field (8) is understood in the sense of distributions: it features a surface distribution on Γ since $\nabla I_s = \delta_\Gamma \boldsymbol{n}_{fs}$ where δ_Γ is the Dirac surface distribution of Γ and $\boldsymbol{n}_{fs}$ the unit normal to Γ oriented from the fluid to the solid. Due to the surface distribution of $\boldsymbol{f}$ on Γ, $\boldsymbol{\sigma}$ is discontinuous across Γ with a jump of the stress vector equal to $(\boldsymbol{\sigma}_{|f} + (\boldsymbol{F}\cdot\boldsymbol{x})\mathbf{1}) \cdot \boldsymbol{n}_{fs}$. When the field (8) is used in problem (7), it comes in Ω_s that the stress is $-(\boldsymbol{F}\cdot\boldsymbol{x})\mathbf{1}$ which is compatible with zero velocity.

By linearity of problem (7), the fields $\boldsymbol{v}$ and $\boldsymbol{f}$ linearly depends on $\boldsymbol{F}$ via some force concentration tensor field $\boldsymbol{\kappa}$ and $\boldsymbol{b}$ such that:

$$\forall \boldsymbol{x} \in \Omega, \quad \boldsymbol{v}(\boldsymbol{x}) = -\frac{1}{\mu}\boldsymbol{\kappa}(\boldsymbol{x}) \cdot \boldsymbol{F} \text{ with } \overline{\boldsymbol{\kappa}}^{\Omega} = \boldsymbol{k}_{\text{hom}} \quad ; \quad \boldsymbol{f}(\boldsymbol{x}) = \boldsymbol{b}(\boldsymbol{x}) \cdot \boldsymbol{F} \text{ with } \overline{\boldsymbol{b}}^{\Omega} = \mathbf{1} \tag{9}$$

As $\boldsymbol{f}$, the force concentration field $\boldsymbol{b}$ has a surface distribution term at Γ. When the macroscopic velocity $\boldsymbol{V}$ is chosen as the loading parameter instead of $\boldsymbol{F}$, concentration tensor fields are similarly defined as:

$$\forall \boldsymbol{x} \in \Omega, \quad \boldsymbol{v}(\boldsymbol{x}) = \boldsymbol{a}(\boldsymbol{x}) \cdot \boldsymbol{V} \text{ with } \overline{\boldsymbol{a}}^{\Omega} = \mathbf{1} \quad ; \quad \boldsymbol{f}(\boldsymbol{x}) = -\mu\boldsymbol{\rho}(\boldsymbol{x}) \cdot \boldsymbol{V} \text{ with } \overline{\boldsymbol{\rho}}^{\Omega} = \boldsymbol{r}_{\text{hom}} \tag{10}$$

where $\boldsymbol{r}_{\text{hom}} = \boldsymbol{k}_{\text{hom}}^{-1}$ is the homogenized resistance, $\boldsymbol{\kappa} = \boldsymbol{a} \cdot \boldsymbol{k}_{\text{hom}}$ and $\boldsymbol{b} = \boldsymbol{\rho} \cdot \boldsymbol{k}_{\text{hom}}$.

The homogenized permeability $\boldsymbol{k}_{\text{hom}}$ (5) or resistance $\boldsymbol{r}_{\text{hom}}$ can hence be computed from the region-wise averages $\overline{\boldsymbol{\kappa}}^{i}$ or $\overline{\boldsymbol{\rho}}^{i}$ via the decomposition (6). The aim of the article is to derive a strategy to *estimate* $\overline{\boldsymbol{\kappa}}^{i}$ or $\overline{\boldsymbol{\rho}}^{i}$ in each region Ω_i from an appropriate choice of an inhomogeneity problem which features a single Morphological Representative Pattern (MRP) embedded in a homogenenous medium, akin to generalized Eshelby problems for linear elasticity in continuum micromechanics [6, 70].

3. Brinkman inhomogeneity and cell problems

Brinkman inhomogeneity problems are *auxiliary* problems introduced as building blocks for the construction of *estimates* to the region-wise averages $\overline{\boldsymbol{\kappa}}^i$ or $\overline{\boldsymbol{\rho}}^i$ of the concentration tensors of P_{Stokes}. An inhomogeneity problem features a single inhomogeneity or MRP surrounded by a homogeneous porous medium. The final estimates of $\overline{\boldsymbol{\kappa}}^i$ or $\overline{\boldsymbol{\rho}}^i$ – and thus of the homogenized permeability – will result from the combination of concentration tensors defined on the inhomogeneity problems in this section using various homogenization schemes exposed in section 4. In these auxiliary problems, Brinkman equations are used following the strategy by [52–57, 60, 66]. The originality of the present section lies (1) in the arbitrary types of inhomogeneities which are considered, including inhomogeneities which represent only some types of pores or solid grains, a multi-layered grain surrounded by a fluid envelope, or any idea relevant to the microstructure to be modelled, (2) in the definition and study of property contribution tensors and equivalent apparent properties which allow a generic treatment in view of the homogenization schemes presented in section 4.

Since the mathematical treatment of the *inhomogeneity* problems is close to that of *cell* problems which are used to build cell models (see section 1), we also take advantage of the developments in this section to highlight some useful properties of the cell problems.

3.1. Brinkman's equation

To study the drag force experienced by a solid particle in a swarm, Brinkman [60] suggested describing the flow through a swarm of fixed particles by introducing a drag force term proportional to the velocity in the momentum balance equation of a Stokes fluid:

$$-\boldsymbol{\nabla} p + \mu' \Delta \boldsymbol{v} - \mu \boldsymbol{k}^{-1} \cdot \boldsymbol{v} = 0 \tag{11}$$

Brinkman's equation (11) can be viewed as an ensemble average of the momentum balance equation of (7) over random realizations of the microstructure seen as a random field. The force $-\mu \boldsymbol{k}^{-1} \cdot \boldsymbol{v}$ accounts for the expectation of the force field $\boldsymbol{f}$ exerted by the solid on the fluid. Brinkman [60] introduced the effective viscosity μ' to account for a possible modification of momentum transport by the solid phase.

The relation between the Stokes to Darcy upscaling problem and Brinkman equations has been investigated by several techniques. When the medium is statistically homogeneous, Brinkman equations can only arise for dilute concentrations of solid particles under specific constraint between the particle size and the solid concentration [63–65, 71–77]. Otherwise, Darcy equations prevail in a statistically homogeneous porous medium with non-dilute solid concentration, even for a poor separation of the macroscopic and pore scales [76]. In turn, when the medium is *not* statistically homogeneous and with poor separation of scales, a Brinkman-like term arises [58, 61, 62, 78] as a higher order corrective term, even for non-dilute solid concentrations.

By definition, an inhomogeneity problem attempts to account for a statistically non-homogeneous flow. Indeed, it aims at estimating the concentration of fields of the conditional ensemble average of the flow past patterns of a region Ω_i. By conditional average, we mean that there always is a pattern of region Ω_i at the center of the averaged problems, which can be obtained by suitable translations of P_{Stokes}. For statistically homogeneous disordered media, the conditional average of the properties far from the center should be homogeneous. This heuristically motivates the use of Brinkman equations in the inhomogeneity problems, with an inhomogeneity embedded in an otherwise homogeneous domain.

3.2. Restrictive assumptions on the effective viscosity and the continuity of the fields

Effective viscosity. The effective viscosity concept has been investigated by theoretical [58, 65, 79–81] or numerical [82] means. Recently, [62] suggested extending the effective viscosity notion to a fourth-rank symmetric anisotropic viscosity tensor in the fluid constitutive law. As of today, there seem to be no consensus whether the ratio μ'/μ should be greater [58, 60, 65, 79, 82] or smaller [60, 80, 81] than 1. This point, which may be microstructure dependent, is not investigated in the present contribution. In the absence of a practical tool to estimate μ' for any microstructure type, we assume $\mu' = \mu$ throughout the remainder of the document. This is acknowledged as a limitation and an open issue.

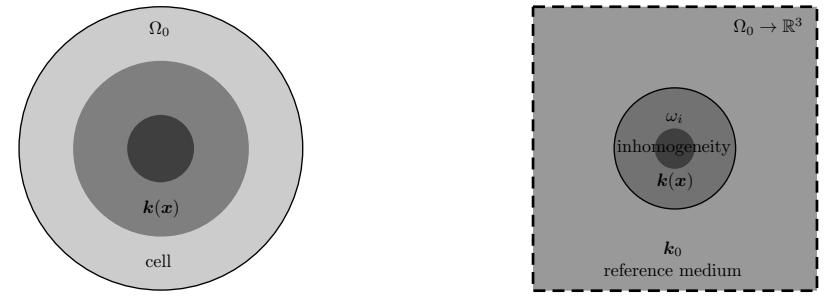

(a) a cell problem (b) an inhomogeneity problem

Figure 2: Examples of cell and inhomogeneity problems with different types of boundary conditions (PBC can only be used when Ω_0 is a parallelepiped). (a) the whole domain Ω_0 is a cell of heterogeneous permeability $\boldsymbol{k}(\boldsymbol{x})$ whose apparent permeability $\boldsymbol{k}_{\text{app}}$ is used to estimate $\boldsymbol{k}_{\text{hom}}$; (b) the inhomogeneity ω_i is a morphologically representative pattern of a region Ω_i of the RVE, embedded in a reference medium of uniform permeability $\boldsymbol{k}_0$.

Continuity of the fields. The continuity of the fields at the clear fluid – porous medium interface has been extensively studied (see e.g. [58, 59, 62, 65, 83–85]), pointing out the need to introduce a jump in the stress across the interface to account for momentum transfer. Such jump condition has been accounted for in the cell and inhomogeneity problems in [50, 51, 57].

In our quest to the construction of a methodology to quickly estimate the homogenized permeability from a restricted set of microstructure parameters, we face two issues. The first issue is that the jump condition introduces an additional parameter (which can be positive or negative in the case of the jump condition by [59]) whose dependence on the microstructure characteristics is not known *a priori* and which is usually fitted. Accounting for it would thus impair the use of the methodology as a predictive tool. The second issue is that the generalization of the jump condition to the interface between two distinct *arbitrary* porous phases would be required to properly account for momentum transfer at interfaces in the heterogeneous Brinkman problem (13). Such generalized jump condition is yet unavailable to the best of our knowledge. For these two reasons, we restrict our study to the case of continuity of the stress vector $\boldsymbol{\sigma}\cdot\boldsymbol{n}$ across interfaces, where $\boldsymbol{n}$ is the unit normal to the interface. This is acknowledged has another current limitation.

Accordingly, admissible velocity and stress field are here assumed to belong to the following continuity sets:

$$\begin{aligned} \mathcal{C}_{\boldsymbol{v}} &= \{\boldsymbol{v}\,|\text{continuous}\ ;\ \nabla\cdot\boldsymbol{v} = 0\,\} \\ \mathcal{C}_{\boldsymbol{\sigma}} &= \{\boldsymbol{\sigma}\,|\boldsymbol{\sigma}\cdot\boldsymbol{n}\ \text{continuous across any surface of discontinuity with normal}\ \boldsymbol{n}\,\} \end{aligned} \tag{12}$$

3.3. Generic heterogeneous Brinkman problem definition

The generic heterogeneous Brinkman problem is defined on a domain Ω_0 in which the permeability $\boldsymbol{k}$ is a heterogeneous tensor field (see figure 2). This generic heterogeneous problem will allow the study of both:

- *cell problems* P_{cell} (fig. 2a): the whole cell Ω_0 represents all the regions of the RVE Ω in a simplified way to keep solutions of P_{cell} tractable analytically or semi-analytically.
- *inhomogeneity problems* $P_{i,0}^{\text{inhom}}$ (fig. 2b): The domain Ω_0 is arbitrarily large and contains a single inhomogeneity that occupies a domain $\omega_i \subset \Omega_0$. The domain ω_i is chosen as a MRP of patterns of a region Ω_i chosen in (6) for each $i \in \{1,\dots,n\}$. The permeability field of $P_{i,0}^{\text{inhom}}$ is equal to some uniform reference permeability $\boldsymbol{k}_0$ for the reference medium in $\Omega_0\backslash\omega_i$ but can be arbitrarily heterogeneous within the inhomogeneity ω_i. Of course, simple shapes must be used when one wishes to keep solutions to $P_{i,0}^{\text{inhom}}$ tractable analytically or semi-analytically for computational efficiency reasons.

Field equations. The generic heterogeneous Brinkman problem is defined as:

$$\nabla \cdot \boldsymbol{\sigma} + \boldsymbol{f} = 0 \qquad \text{in } \Omega_0 \tag{13a}$$
$$\boldsymbol{f} = -\mu \boldsymbol{k}^{-1} \cdot \boldsymbol{v} \qquad \text{in } \Omega_0 \tag{13b}$$
$$\boldsymbol{\sigma} = -p\mathbf{1} + 2\mu \nabla^s \boldsymbol{v} \qquad \text{in } \Omega_0 \tag{13c}$$
$$\nabla \cdot \boldsymbol{v} = 0 \qquad \text{in } \Omega_0 \tag{13d}$$
$$\boldsymbol{v} \text{ and } p - \boldsymbol{F}_0 \cdot \boldsymbol{x} \text{ periodic} \qquad \text{on } \partial\Omega_0 \text{ if PBC} \tag{13e}$$
$$\boldsymbol{v} = \boldsymbol{V}_0 \qquad \text{on } \partial\Omega_0 \text{ if KUBC} \tag{13f}$$
$$\boldsymbol{\sigma} \cdot \boldsymbol{n} = -(\boldsymbol{F}_0 \cdot \boldsymbol{x})\boldsymbol{n} \qquad \text{on } \partial\Omega_0 \text{ if SUBC} \tag{13g}$$

where $\boldsymbol{n}$ is the outward unit normal to $\partial\Omega_0$. The field $\boldsymbol{f}$ is a body force which accounts for the resisting efforts via the Brinkman term. The combination of (13a), (13b) and (13c) yields Brinkman's momentum equation:

$$-\boldsymbol{\nabla} p + \mu \Delta \boldsymbol{v} - \mu \boldsymbol{k}^{-1} \cdot \boldsymbol{v} = 0 \tag{14}$$

The loading parameters $\boldsymbol{F}_0$ or $\boldsymbol{V}_0$ are uniform vectors, interpreted respectively as a body force or a velocity. Three variants in boundary conditions are investigated: periodic (PBC), kinematically uniform (KUBC) or statically uniform (SUBC) boundary conditions. The boundary conditions early investigated in the cell problem of Cunningham [40] correspond to KUBC. Alternative types of boundary conditions sometimes used for cell problems such as the zero vorticity one [46], the zero shear stress–uniform normal velocity one [41–44] or the Kvashnin [86] one are not considered. For isotropic local permeabilities and cylindrical or spherical geometries, Brinkman equation admits separable solution and the zero shear stress–uniform normal velocity boundary condition appears to coincide with SUBC (see Appendix A) ; however, they can differ in general.

Heterogeneous Brinkman problems have been addressed by numerical methods in e.g. [67]. The permeability field $\boldsymbol{k}$ – or its inverse the resistance field $\boldsymbol{r} = \boldsymbol{k}^{-1}$ – is here arbitrary. Extreme permeability values are locally allowed, which namely correspond to:

- clear fluid when $\boldsymbol{r} = 0$ ($\boldsymbol{k} \to \infty$): since $\boldsymbol{f} = 0$, eq. (14) becomes $-\boldsymbol{\nabla} p + \mu \Delta \boldsymbol{v}$ which is Stokes' momentum equation for a Newtonian fluid ;
- solid when $\boldsymbol{k} = 0$: the velocity is then $\boldsymbol{v} = 0$ and the body force $\boldsymbol{f}$ is locally indeterminate. In that case, only the resultant force exerted by a solid region ω_s is known by $\int_{\omega_s} \boldsymbol{f} \, \mathrm{d}V = -\int_{\partial\omega_s} \boldsymbol{\sigma} \cdot \boldsymbol{n} \, \mathrm{d}S$ from (13a) and the divergence theorem.

Admissible fields. For SUBC, KUBC or PBC, the sets of velocity fields kinematically admissible with some uniform velocity $\boldsymbol{V}_0$ and stress fields statically admissible with some uniform drag force density $\boldsymbol{F}_0$ specify as:

$$\begin{array}{|r|l}
\multirow{2}{*}{KUBC} & \mathcal{K}(\boldsymbol{V}_0) = \{\boldsymbol{v} \in \mathcal{C}_{\boldsymbol{v}} \,|\boldsymbol{v} = \boldsymbol{V}_0 \text{ on } \partial\Omega_0\} \\
& \mathcal{S}(\boldsymbol{F}_0) = \left\{\boldsymbol{\sigma} \in \mathcal{C}_{\boldsymbol{\sigma}} \,\middle|\, \frac{1}{|\Omega_0|}\int_{\partial\Omega_0} \boldsymbol{\sigma} \cdot \boldsymbol{n} \, \mathrm{d}S = -\boldsymbol{F}_0 \right\} \\
\multirow{2}{*}{SUBC} & \mathcal{K}(\boldsymbol{V}_0) = \left\{\boldsymbol{v} \in \mathcal{C}_{\boldsymbol{v}} \,\middle|\, \frac{1}{|\Omega_0|}\int_{\partial\Omega_0} \boldsymbol{x}\,(\boldsymbol{v} \cdot \boldsymbol{n}) \, \mathrm{d}S = \boldsymbol{V}_0 \right\} \\
& \mathcal{S}(\boldsymbol{F}_0) = \{\boldsymbol{\sigma} \in \mathcal{C}_{\boldsymbol{\sigma}} \,|\boldsymbol{\sigma} \cdot \boldsymbol{n} = -(\boldsymbol{F}_0 \cdot \boldsymbol{x})\boldsymbol{n} \text{ on } \partial\Omega_0\} \\
\multirow{2}{*}{PBC} & \mathcal{K}(\boldsymbol{V}_0) = \{\boldsymbol{v} \in \mathcal{C}_{\boldsymbol{v}} \,|\boldsymbol{v} \text{ periodic on } \partial\Omega_0 \text{ and } \overline{\boldsymbol{v}}_0^{\Omega} = \boldsymbol{V}_0\} \\
& \mathcal{S}(\boldsymbol{F}_0) = \{\boldsymbol{\sigma} \in \mathcal{C}_{\boldsymbol{\sigma}} \,|\boldsymbol{\sigma} \cdot \boldsymbol{n} + (\boldsymbol{F}_0 \cdot \boldsymbol{x})\boldsymbol{n} \text{ anti-periodic on } \partial\Omega_0\}
\end{array} \tag{15}$$

For each of the above types of boundary conditions, the relaxed set $\mathcal{K} = \cup_{\boldsymbol{V}_0 \in \mathbb{R}^3} \mathcal{K}(\boldsymbol{V}_0)$ (resp. $\mathcal{S} = \cup_{\boldsymbol{F}_0 \in \mathbb{R}^3} \mathcal{S}(\boldsymbol{F}_0)$) is defined when the imposed load is the force $\boldsymbol{F}_0$ (resp. the velocity $\boldsymbol{V}_0$).

Velocity or force control. The flow in the generic heterogeneous Brinkman problem (13) is driven by imposing either the uniform velocity $\boldsymbol{V}_0$ or the uniform body force $\boldsymbol{F}_0$. The flow problem is generically defined for each type of boundary condition from the field equations (13a) through (13d) together with one of the two following types of controls:

$$\text{velocity control:} \quad \boldsymbol{v} \in \mathcal{K}(\boldsymbol{V}_0) \text{ and } \boldsymbol{\sigma} \in \mathcal{S} \qquad ; \qquad \text{force control :} \quad \boldsymbol{v} \in \mathcal{K} \text{ and } \boldsymbol{\sigma} \in \mathcal{S}(\boldsymbol{F}_0) \tag{16}$$

Virtual power theorem. Admissible fields enjoy the following virtual power theorem in KUBC, SUBC or PBC:

$$\forall \boldsymbol{v}' \in \mathcal{K}(\boldsymbol{V}_0') \ , \ \forall \boldsymbol{\sigma} \in \mathcal{S}(\boldsymbol{F}_0) \qquad \mathcal{P}(\boldsymbol{v}', \boldsymbol{\sigma}) := \int_{\Omega_0} \left[(\nabla^s \boldsymbol{v}') : \boldsymbol{\sigma} + \boldsymbol{v}' \cdot (\nabla \cdot \boldsymbol{\sigma}) \right] \mathrm{d}V = -|\Omega_0| \boldsymbol{V}_0' \cdot \boldsymbol{F}_0 \tag{17}$$

Indeed, the term within the square brackets is $\nabla \cdot (\boldsymbol{v}' \cdot \boldsymbol{\sigma})$ thus $\mathcal{P}(\boldsymbol{v}', \boldsymbol{\sigma}) = \int_{\partial\Omega_0} \boldsymbol{v}' \cdot \boldsymbol{\sigma} \cdot \boldsymbol{n} \, \mathrm{d}S$ by direct application of the divergence theorem. The final equality in (17) results from the properties of the different sets of boundary conditions. As a side note, theorem (17) would not apply to the zero vorticity boundary condition used by [46].

Averaging rules. The velocity $\boldsymbol{V}_0$ and the body force $\boldsymbol{F}_0$ respectively correspond to the volume average of the fields $\boldsymbol{v}$ and $\boldsymbol{f}$ from (15) and (17):

$$\begin{aligned} \boldsymbol{V}_0 &= \frac{1}{|\Omega_0|} \int_{\partial\Omega_0} \boldsymbol{x} (\boldsymbol{v} \cdot \boldsymbol{n}) \, \mathrm{d}S \quad &= \overline{\boldsymbol{v}}^{\Omega_0} = -\tfrac{1}{\mu} \overline{\boldsymbol{k} \cdot \boldsymbol{f}}^{\Omega_0} \\ \boldsymbol{F}_0 &= -\frac{1}{|\Omega_0|} \int_{\partial\Omega_0} \boldsymbol{\sigma} \cdot \boldsymbol{n} \, \mathrm{d}S \quad &= \overline{\boldsymbol{f}}^{\Omega_0} = -\mu \overline{\boldsymbol{r} \cdot \boldsymbol{v}}^{\Omega_0} \end{aligned} \tag{18}$$

Concentration tensors. Under velocity control (resp. force control), by linearity of the problem (13), the solution velocity (resp. force) is linearly related to $\boldsymbol{V}_0$ (resp. $\boldsymbol{F}_0$) by some velocity concentration tensor field $\boldsymbol{A}$ (resp. force concentration $\boldsymbol{B}$) such as at any point $\boldsymbol{x}$ of the domain Ω_0:

$$\boldsymbol{v}(\boldsymbol{x}) = \boldsymbol{A}(\boldsymbol{x}) \cdot \boldsymbol{V}_0 \text{ with } \overline{\boldsymbol{A}}^{\Omega_0} = \boldsymbol{1} \quad \text{(velocity control)} \quad ; \quad \boldsymbol{f}(\boldsymbol{x}) = \boldsymbol{B}(\boldsymbol{x}) \cdot \boldsymbol{F}_0 \text{ with } \overline{\boldsymbol{B}}^{\Omega_0} = \boldsymbol{1} \quad \text{(force control)} \tag{19}$$

where the identity $\boldsymbol{1}$ result from the averaging rules (18) and properties of admissible fields for all types of BCs. Provided $\boldsymbol{k}_0$ is non-null and finite, the velocity and force concentration tensors are related by

$$\boldsymbol{k} \cdot \boldsymbol{B} = \boldsymbol{A} \cdot \boldsymbol{k}_0 \tag{20}$$

3.4. Cell problems

Let us first focus on cell problems P_{cell} in which Ω_0 is a cell which represents all regions of the RVE in a simplified way (fig. 2a). The averaging rules (18) provide a motivation to interpret $\boldsymbol{V}_0$ and $\boldsymbol{F}_0$ as estimates to the macroscopic variables $\boldsymbol{V}$ and $\boldsymbol{F}$ introduced in sec. 2 and (19) is reminiscent of (9), (10).

Apparent properties of the cell. From (18) and (19), apparent permeability $\boldsymbol{k}_{\text{app}}$ and resistance $\boldsymbol{r}_{\text{app}} = \boldsymbol{k}_{\text{app}}^{-1}$ of the cell Ω_0 are defined as:

$$\boldsymbol{r}_{\text{app}} = \overline{\boldsymbol{r} \cdot \boldsymbol{A}}^{\Omega_0} \quad \text{(velocity control)} \qquad ; \qquad \boldsymbol{k}_{\text{app}} = \overline{\boldsymbol{k} \cdot \boldsymbol{B}}^{\Omega_0} \quad \text{(force control)} \tag{21}$$

Since $\boldsymbol{V}_0 = -\frac{1}{\mu} \boldsymbol{k}_{\text{app}} \cdot \boldsymbol{F}_0$, the apparent permeability of the cell is used as an *estimate* to the homogenized permeability $\boldsymbol{k}_{\text{hom}}$ (5) in most *cell models* cited in sec. 1. In general, the concentration tensors $\boldsymbol{A}$ and $\boldsymbol{B}$ and hence the apparent properties $\boldsymbol{k}_{\text{app}} = \boldsymbol{r}_{\text{app}}^{-1}$ depend on the type of boundary conditions (PBC, KUBC or SUBC), see e.g. (27).

Symmetry of $\boldsymbol{r}_{\text{app}}$ or $\boldsymbol{k}_{\text{app}}$ follows from the virtual power theorem (17). Let $(\boldsymbol{v}, \boldsymbol{\sigma})$ (resp. $(\boldsymbol{v}', \boldsymbol{\sigma}')$) the solutions to the generic Brinkman problem (13) under velocity control with velocity $\boldsymbol{V}_0$ (resp. $\boldsymbol{V}_0'$), then from (17)

$$|\Omega_0| \boldsymbol{V}_0' \cdot \mu \, \boldsymbol{r}_{\text{app}} \cdot \boldsymbol{V}_0 = -\mathcal{P}(\boldsymbol{v}', \boldsymbol{\sigma}) = -\mathcal{P}(\boldsymbol{v}, \boldsymbol{\sigma}') = |\Omega_0| \boldsymbol{V}_0 \cdot \mu \, \boldsymbol{r}_{\text{app}} \cdot \boldsymbol{V}_0' \tag{22}$$

which shows the symmetry, irrespective of the type of boundary conditions investigated here.

Energy theorems. The kinematic energy functional W defined on velocities and the complementary static energy functional W^* defined on stresses are introduced as:

$$\begin{aligned} W(\boldsymbol{v}) &= \int_{\Omega_0} w(\boldsymbol{v})\,\mathrm{d}V \qquad \text{with } w(\boldsymbol{v}) = \tfrac{1}{2}\left[2\mu(\nabla^s\boldsymbol{v}) : (\nabla^s\boldsymbol{v}) + \mu\boldsymbol{v}\cdot\boldsymbol{k}^{-1}\cdot\boldsymbol{v}\right] \\ W^*(\boldsymbol{\sigma}) &= \int_{\Omega_0} w^*(\boldsymbol{\sigma})\,\mathrm{d}V \qquad \text{with } w^*(\boldsymbol{\sigma}) = \tfrac{1}{2}\left[\tfrac{1}{2\mu}\boldsymbol{\sigma}_{\mathrm{dev}} : \boldsymbol{\sigma}_{\mathrm{dev}} + \tfrac{1}{\mu}(\boldsymbol{\nabla}\cdot\boldsymbol{\sigma})\cdot\boldsymbol{k}\cdot(\boldsymbol{\nabla}\cdot\boldsymbol{\sigma})\right] \end{aligned} \tag{23}$$

where $\boldsymbol{\sigma}_{\mathrm{dev}} = \boldsymbol{\sigma} - \frac{1}{3}(\boldsymbol{\sigma} : \mathbf{1})\mathbf{1}$ is the deviatoric stress. Since the functionals W and W^* are positive definite quadratic forms, repeated use of the virtual power theorem (17) and definitions (23) classically yields the following minimum energy theorems:

$$\begin{aligned} \frac{|\Omega_0|}{2}\mu\boldsymbol{V}_0\cdot\boldsymbol{r}_{\mathrm{app}}\cdot\boldsymbol{V}_0 &= \inf_{\boldsymbol{u}\in\mathcal{K}(\boldsymbol{V}_0)} W(\boldsymbol{u}) \qquad = -\inf_{\boldsymbol{\sigma}'\in\mathcal{S}}(W^*-\Phi^*)(\boldsymbol{\sigma}',\boldsymbol{V}_0) \qquad \text{(velocity control)} \\ \frac{|\Omega_0|}{2\mu}\boldsymbol{F}_0\cdot\boldsymbol{k}_{\mathrm{app}}\cdot\boldsymbol{F}_0 &= \inf_{\boldsymbol{\sigma}'\in\mathcal{S}(\boldsymbol{F}_0)} W^*(\boldsymbol{\sigma}') \qquad = -\inf_{\boldsymbol{u}\in\mathcal{K}}(W-\Phi)(\boldsymbol{u},\boldsymbol{F}_0) \qquad \text{(force control)} \end{aligned} \tag{24}$$

where the virtual powers of external given loads are defined on admissible fields as:

$$\Phi(\boldsymbol{u},\boldsymbol{F}_0) = -\boldsymbol{F}_0\cdot\int_{\partial\Omega_0}\boldsymbol{x}(\boldsymbol{u}\cdot\boldsymbol{n})\,\mathrm{d}S \quad \text{(force control)} \quad ; \quad \Phi^*(\boldsymbol{\sigma}',\boldsymbol{V}_0) = \boldsymbol{V}_0\cdot\int_{\partial\Omega_0}\boldsymbol{\sigma}'\cdot\boldsymbol{n}\,\mathrm{d}V \quad \text{(velocity control)} \tag{25}$$

The minimum energy theorems (24) provide energy definitions to the apparent properties and means to construct bounds on them. For example, since $\boldsymbol{v} = \boldsymbol{V}_0 \in \mathcal{K}(\boldsymbol{V}_0)$ and $\boldsymbol{\sigma} = -(\boldsymbol{F}_0\cdot\boldsymbol{x})\mathbf{1} \in \mathcal{S}(\boldsymbol{F}_0)$ for all types of boundary conditions, the apparent properties are bounded by analogues to the Voigt and Reuss bounds:

$$\boldsymbol{k}_{\mathrm{app}} \le \overline{\boldsymbol{k}}^{\Omega_0} \quad ; \quad \boldsymbol{r}_{\mathrm{app}} \le \overline{\boldsymbol{r}}^{\Omega_0} \tag{26}$$

where inequalities stand in the sense of positive definite quadratic forms. Further, since $\mathcal{K}^{\mathrm{KUBC}}(\boldsymbol{V}_0) \subset \mathcal{K}^{\mathrm{PBC}}(\boldsymbol{V}_0)$ and $\mathcal{S}^{\mathrm{SUBC}}(\boldsymbol{F}_0) \subset \mathcal{S}^{\mathrm{PBC}}(\boldsymbol{F}_0)$, one may easily prove from (24) the hierarchy:

$$\boldsymbol{k}_{\mathrm{app}}^{\mathrm{KUBC}} \le \boldsymbol{k}_{\mathrm{app}}^{\mathrm{PBC}} \le \boldsymbol{k}_{\mathrm{app}}^{\mathrm{SUBC}} \tag{27}$$

3.5. Inhomogeneity problems

In an inhomogeneity problem $P_{i,0}^{\mathrm{inhom}}$, the domain Ω_0 is arbitrarily large and contains a single inhomogeneity that occupies a domain $\omega_i \subset \Omega_0$ (see figure 2b). Akin to Eshelby's inhomogeneity problem in linear elasticity [6], we consider the asymptotic case where $\Omega_0 \to \mathbb{R}^3$. In that case, provided the inhomogeneity ω_i is of finite extension, PBC, KUBC and SUBC coincide as the far field in the reference material asymptotically verifies:

$$\text{as } |\boldsymbol{x}| \to \infty : \qquad \boldsymbol{v} \to \boldsymbol{V}_0 \quad ; \quad \boldsymbol{\sigma} \sim -(\boldsymbol{F}_0\cdot\boldsymbol{x})\mathbf{1} \quad ; \quad \boldsymbol{f} = -\boldsymbol{\nabla}\cdot\boldsymbol{\sigma} \to \boldsymbol{F}_0 \tag{28}$$

To handle mathematical difficulties related to the definition of a flow problem in a infinite domain, the admissible sets $\mathcal{K}(\boldsymbol{V}_0)$ and $\mathcal{S}(\boldsymbol{F}_0)$ (15) are restricted to velocity and stress fields that have a square integrable deviation from the uniform asymptotic behavior (28). More precisely, the incremental energy densities $w(\boldsymbol{v}-\boldsymbol{V}_0)$ and $w^*(\boldsymbol{\sigma}+(\boldsymbol{F}_0\cdot\boldsymbol{x})\mathbf{1})$ must be integrable on $\mathbb{R}^3$, where w and w^* are defined in (23).

Average concentration tensor. The averages over the inhomogeneity ω_i of the concentration tensors (19) are of paramount importance to the methodology and denoted:

$$\boldsymbol{A}_{i,0} := \overline{\boldsymbol{A}}^{\omega_i} \quad \text{(velocity control)} \qquad ; \qquad \boldsymbol{B}_{i,0} := \overline{\boldsymbol{B}}^{\omega_i} \quad \text{(force control)} \tag{29}$$

Equivalent properties. Apparent or equivalent permeability $\boldsymbol{k}_{i,0}$ and resistance $\boldsymbol{r}_{i,0} = \boldsymbol{k}_{i,0}^{-1}$ of the inhomogeneity ω_i embedded in a reference medium with permeability $\boldsymbol{k}_0$ are defined as:

$$\boldsymbol{r}_{i,0} := \overline{\boldsymbol{r}\cdot\boldsymbol{A}}^{\omega_i}\cdot\left(\overline{\boldsymbol{A}}^{\omega_i}\right)^{-1} \quad \text{(velocity control)} \qquad ; \qquad \boldsymbol{k}_{i,0} := \overline{\boldsymbol{k}\cdot\boldsymbol{B}}^{\omega_i}\cdot\left(\overline{\boldsymbol{B}}^{\omega_i}\right)^{-1} \quad \text{(force control)} \tag{30}$$

From (13b) and (19), the normalization by $\boldsymbol{A}_{i,0}$ or $\boldsymbol{B}_{i,0}$ in (30) indeed ensures:

$$\overline{\boldsymbol{f}}^{\omega_i} = -\mu\,\boldsymbol{r}_{i,0}\cdot\overline{\boldsymbol{v}}^{\omega_i} \quad \text{(velocity control)} \qquad ; \qquad \overline{\boldsymbol{v}}^{\omega_i} = -\tfrac{1}{\mu}\,\boldsymbol{k}_{i,0}\cdot\overline{\boldsymbol{f}}^{\omega_i} \quad \text{(force control)} \tag{31}$$

In the case of infinite resistance (i.e. a solid inhomogeneity), the average drag force density $\overline{\boldsymbol{f}}^{\omega_i} = -\mu\overline{\boldsymbol{r}\cdot\boldsymbol{v}}^{\omega_i}$ involves the volume integral of an indeterminate term as $\boldsymbol{v}$ vanishes, so that the alternative expression is preferred:

$$\overline{\boldsymbol{f}}^{\omega_i} = -\mu\overline{\boldsymbol{r}\cdot\boldsymbol{A}}^{\omega_i}\cdot\boldsymbol{V}_0 = \frac{1}{|\omega_i|}\int_{\partial\omega_i}\boldsymbol{\sigma}\cdot\boldsymbol{n}\,\mathrm{d}S \tag{32}$$

The equivalent properties $\boldsymbol{k}_{i,0} = \boldsymbol{r}_{i,0}^{-1}$ depend on the reference medium permeability $\boldsymbol{k}_0$ in general. Unlike the apparent properties $\boldsymbol{k}_{\text{app}} = \boldsymbol{r}_{\text{app}}^{-1}$ defined in (21) for cells problems, the symmetry of the equivalent properties of the inhomogeneity cannot be shown in general.

Property contribution tensors. The replacement of the reference medium property $\boldsymbol{k}_0 = \boldsymbol{r}_0^{-1}$ by some (possibly heterogeneous) property $\boldsymbol{k} = \boldsymbol{r}^{-1}$ in the inhomogeneity ω_i induces a flow perturbation from the undisturbed fields which correspond to the asymptotic fields of (28).

Let $(\boldsymbol{v},\boldsymbol{\sigma})$ and $(\boldsymbol{v}',\boldsymbol{\sigma}')$ the solutions to the inhomogeneity problem under velocity control (resp. force control) with imposed velocities $\boldsymbol{V}_0$ and $\boldsymbol{V}_0'$ (resp. forces $\boldsymbol{F}_0$ and $\boldsymbol{F}_0'$). The crossed power increment induced by the replacement of the reference medium by the inhomogeneity is:

$$\delta\mathcal{P}_0(\boldsymbol{v}',\boldsymbol{\sigma}) := \begin{cases}\displaystyle\int_{\mathbb{R}^3}\left[(\nabla^s\boldsymbol{v}'):\boldsymbol{\sigma}+\boldsymbol{v}'\cdot(\nabla\cdot\boldsymbol{\sigma})-\mu\boldsymbol{V}_0'\cdot\boldsymbol{r}_0\cdot\boldsymbol{V}_0\right]\mathrm{d}V & \text{(velocity control)}\\ \displaystyle\int_{\mathbb{R}^3}\left[(\nabla^s\boldsymbol{v}'):\boldsymbol{\sigma}+\boldsymbol{v}'\cdot(\nabla\cdot\boldsymbol{\sigma})-\tfrac{1}{\mu}\boldsymbol{F}_0'\cdot\boldsymbol{k}_0\cdot\boldsymbol{F}_0\right]\mathrm{d}V & \text{(force control)}\end{cases} \tag{33}$$

Application of the virtual power theorem (17) to (33) yields:

$$\begin{aligned}\delta\mathcal{P}_0(\boldsymbol{v}',\boldsymbol{\sigma}) &= \boldsymbol{V}_0'\cdot\int_{\mathbb{R}^3}\mu(\boldsymbol{r}\cdot\boldsymbol{v}-\boldsymbol{r}_0\cdot\boldsymbol{V}_0)\,\mathrm{d}V = \boldsymbol{V}_0'\cdot\int_{\mathbb{R}^3}\mu\left[\boldsymbol{r}_0\cdot(\boldsymbol{v}-\boldsymbol{V}_0)+\mu(\boldsymbol{r}-\boldsymbol{r}_0)\cdot\boldsymbol{v}\right]\mathrm{d}V \qquad \text{(velocity control)}\\ \delta\mathcal{P}_0(\boldsymbol{v}',\boldsymbol{\sigma}) &= \boldsymbol{F}_0'\cdot\int_{\mathbb{R}^3}\tfrac{1}{\mu}(\boldsymbol{k}\cdot\boldsymbol{f}-\boldsymbol{k}_0\cdot\boldsymbol{F}_0)\,\mathrm{d}V = \boldsymbol{F}_0'\cdot\int_{\mathbb{R}^3}\tfrac{1}{\mu}\left[\boldsymbol{k}_0\cdot(\boldsymbol{f}-\boldsymbol{F}_0)+\tfrac{1}{\mu}(\boldsymbol{k}-\boldsymbol{k}_0)\cdot\boldsymbol{f}\right]\mathrm{d}V \qquad \text{(force control)}\end{aligned} \tag{34}$$

The velocity averaging rule implies $\int_{\mathbb{R}^3}\boldsymbol{v}-\boldsymbol{V}_0\,\mathrm{d}V = 0$ while the term $(\boldsymbol{r}-\boldsymbol{r}_0)\cdot\boldsymbol{v}$ is supported in the inhomogeneity ω_i only, and similarly for force control. Resorting to the concentration tensors (19), one has finally:

$$\begin{aligned}\delta\mathcal{P}_0(\boldsymbol{v}',\boldsymbol{\sigma}) &= |\omega_i|\mu\boldsymbol{V}_0'\cdot\overline{(\boldsymbol{r}-\boldsymbol{r}_0)\cdot\boldsymbol{A}}^{\omega_i}\cdot\boldsymbol{V}_0 \qquad \text{(velocity control)}\\ \delta\mathcal{P}_0(\boldsymbol{v}',\boldsymbol{\sigma}) &= |\omega_i|\tfrac{1}{\mu}\boldsymbol{F}_0'\cdot\overline{(\boldsymbol{k}-\boldsymbol{k}_0)\cdot\boldsymbol{B}}^{\omega_i}\cdot\boldsymbol{F}_0 \qquad \text{(force control)}\end{aligned} \tag{35}$$

The quantities in (35) defined by:

$$\boldsymbol{R}_{i,0} := \overline{(\boldsymbol{r}-\boldsymbol{r}_0)\cdot\boldsymbol{A}}^{\omega_i} \quad \text{(velocity control)} \qquad ; \qquad \boldsymbol{K}_{i,0} := \overline{(\boldsymbol{k}-\boldsymbol{k}_0)\cdot\boldsymbol{B}}^{\omega_i} \quad \text{(force control)} \tag{36}$$

are respectively called the *resistance contribution tensor* and *permeability contribution tensor* of the inhomogeneity ω_i surrounded by the reference medium $\boldsymbol{k}_0$, in the spirit of property contribution tensors [5, 87, 88]. It is clear from the reciprocity theorem $\mathcal{P}(\boldsymbol{v}',\boldsymbol{\sigma}) = \mathcal{P}(\boldsymbol{v},\boldsymbol{\sigma}')$ that the property contribution tensors $\boldsymbol{R}_{i,0}$ and $\boldsymbol{K}_{i,0}$ are symmetric (unlike $\boldsymbol{A}_{i,0}$, $\boldsymbol{B}_{i,0}$, $\boldsymbol{k}_{i,0}$ or $\boldsymbol{r}_{i,0}$ in general).

From the definitions (36) and (30), the property contribution tensors are directly expressed from the average concentration tensors $\boldsymbol{A}_{i,0}$ and $\boldsymbol{B}_{i,0}$ (29) in the inhomogeneity by:

$$\boldsymbol{R}_{i,0} = (\boldsymbol{r}_{i,0}-\boldsymbol{r}_0)\cdot\boldsymbol{A}_{i,0} \quad \text{(velocity control)} \qquad ; \qquad \boldsymbol{K}_{i,0} = (\boldsymbol{k}_{i,0}-\boldsymbol{k}_0)\cdot\boldsymbol{B}_{i,0} \quad \text{(force control)} \tag{37}$$

These results hold regardless of the shape of ω_i as well as for arbitrarily heterogeneous permeability within ω_i. When the inhomogeneity ω_i is finite and $\boldsymbol{k}_0 = \boldsymbol{r}_0^{-1}$ are neither zero nor infinite, the permeability and resistance contribution tensors are related by

$$\boldsymbol{K}_{i,0} = -\boldsymbol{k}_0 \cdot \boldsymbol{R}_{i,0} \cdot \boldsymbol{k}_0 \quad \Leftrightarrow \quad \boldsymbol{R}_{i,0} = -\boldsymbol{r}_0 \cdot \boldsymbol{K}_{i,0} \cdot \boldsymbol{r}_0 \tag{38}$$

Physically, the permeability (resp. resistance) contribution tensor relates to the overall permeability (resp. resistance) increment induced by the replacement of the reference medium by the inhomogeneity ω_i. More precisely, let's consider briefly for the sake of illustration that the inhomogeneity problem is not defined on $\mathbb{R}^3$ but on a cell Ω_0 containing ω_i and filled with the reference medium in $\Omega_0 \backslash \omega_i$. Under force control, the apparent permeability $\boldsymbol{k}_{\text{app}}$ of the cell defined by (21) relates to the power increment (33) by $\delta\mathcal{P}_0(\boldsymbol{v}', \boldsymbol{\sigma}) = |\Omega_0| \mu^{-1} \boldsymbol{F}_0' \cdot (\boldsymbol{k}_{\text{app}} - \boldsymbol{k}_0) \cdot \boldsymbol{F}_0$ provided that integrals are performed on Ω_0 instead of $\mathbb{R}^3$ in (33). This allows to link the permeability contribution tensor of the inhomogeneity in the cell to the apparent permeability of the cell by:

$$\boldsymbol{k}_{\text{app}} - \boldsymbol{k}_0 = \varphi \boldsymbol{K}_{i,0}^{\text{inhom. in cell}} \quad \text{(inhomogeneity in cell)} \tag{39}$$

where $\varphi = \frac{|\omega_i|}{|\Omega_0|}$ is the volume fraction of the inhomogeneity ω_i within the cell Ω_0.

As a convenience, we provide in Appendix A the average velocity concentration tensors for spherical (including composite spheres), cylindrical and planar inhomogeneities, for which the Brinkman equations admit separable solutions. These serve as building blocks for the homogenization schemes presented in the next section. When more complex Morphological Representative Patterns are required, the schemes below similarly apply, but one may have to resort to numerical simulation or a semi-analytical strategy to solve the inhomogeneity problems.

4. Homogenization schemes to estimate the homogenized permeability

In this section, several homogenization schemes are presented to estimate the homogenized permeability (5) of the RVE Ω of a porous medium as in sec. 2. To prepare the presentation of these schemes, recall from (9) or (10) that the homogenized permeability and resistance can be indifferently computed by:

$$\begin{aligned} \boldsymbol{r}_{\text{hom}} &= \overline{\boldsymbol{\rho}}^{\Omega} = \sum_i \varphi_i \overline{\boldsymbol{\rho}}^i = \boldsymbol{r}_0 + \sum_i \varphi_i \overline{(\boldsymbol{\rho} - \boldsymbol{r}_0 \cdot \boldsymbol{a})}^i \quad \text{(velocity control)} \\ \boldsymbol{k}_{\text{hom}} &= \overline{\boldsymbol{\kappa}}^{\Omega} = \sum_i \varphi_i \overline{\boldsymbol{\kappa}}^i = \boldsymbol{k}_0 + \sum_i \varphi_i \overline{(\boldsymbol{\kappa} - \boldsymbol{k}_0 \cdot \boldsymbol{b})}^i \quad \text{(force control)} \end{aligned} \tag{40}$$

where $\overline{f}^i$ denotes the volume average of any field f over a region Ω_i with volume fraction $\varphi_i = |\Omega_i|/|\Omega|$ and $\boldsymbol{k}_0 = \boldsymbol{r}_0^{-1}$ is an arbitrary uniform reference property.

The estimates of the homogenized permeability are build from elementary bricks arising from Brinkman inhomogeneity problems to estimate the region-wise averages in (40). Thanks to the general results established in sec. 3, well established ideas of continuum micromechanics on elasticity or conduction homogenization schemes can directly be transposed to the Stokes to Darcy homogenization problem at hand. The purpose of this section is to recall these schemes and adapt them whenever necessary to the present, new context of Brinkman inhomogeneities.

4.1. Choices for the approximate representation of the material by inhomogeneity problems

Decomposition in regions and definition of inhomogeneities. To approximately represent the material, the user of the homogenization schemes must first choose regions Ω_i for the decomposition of the averages in (6) and then inhomogeneities ω_i to represent them. These choices for such approximate representations are usually not unique, although they should be motivated by the actual characteristics of the microstructure of the investigated porous medium. For single porosity material, i.e. when all the heterogeneity have the

same length scale, inhomogeneities have usually a permeability equal either to $\boldsymbol{k} = 0$ (parts of solid) or $\boldsymbol{k} \to \infty$ (pores) or composite inhomogeneities featuring a solid core with $\boldsymbol{k} = 0$ surrounded by a pore shell with $\boldsymbol{k} \to \infty$. For multiple porosity materials, i.e. with pore size spread over several separated length scales, a region Ω_i with a porosity at a scale lower than the current inhomogeneity scale may be represented by an inhomogeneity with a finite, non-zero permeability which would correspond to the homogenized permeability of a RVE of that region only. The apparent permeability of that region could either be known from an experiment on a sample of the material of region Ω_i, full field simulations or a recursive application of the homogenization schemes presented herein at a lower scale. It is also theoretically possible, albeit not practical, to define the permeability of that region Ω_i from the equivalent permeability $\boldsymbol{k}_{i,0}$ (30) of a heterogeneous inhomogeneity directly defined as a representative subset of Ω_i (e.g. with many small pores and solid grains).

In practice, the set of material parameters required for building the estimate comprises: the volume fraction of each region, the shape, size and orientation distribution of each type of inhomogeneity. For actual materials, these information may be inferred from experimental measures such as picnometry (overall porosity), mercury intrusion porosimetry (pore size distribution) or sieve analysis (grain size distribution), analysis with statistical treatment of *many* microscope observations (fiber diameter and orientations, particle shapes, general organisation of the microstructure).

Reference medium. Second, all the presented homogenization schemes rely on the introduction of a reference medium with permeability $\boldsymbol{k}_0$. The choice of $\boldsymbol{k}_0$ varies among schemes, but there are two main categories. In some situations, one region $m \in \{1, \dots, n\}$ among those chosen to decompose the average in (6) plays the specific role of a matrix. This means that only the region Ω_m forms a connected domain in the RVE Ω, while all other regions Ω_i $(i \neq m)$ are constituted of disconnected inclusions embedded in the matrix region. If that region is statistically homogeneous with apparent permeability $\boldsymbol{k}_m$, the choice $\boldsymbol{k}_0 = \boldsymbol{k}_m$ can be made for such *matrix-inclusion* materials. In some other situations, no phase plays the role of a matrix and connectivity of the regions depend on their volume fraction and shape. In that case, the reference medium can be defined as an *effective medium* from the self-consistency requirement $\boldsymbol{k}_0 = \boldsymbol{k}_{\text{hom}}$.

Loading parameters. Third, the auxiliary loading parameters $\boldsymbol{V}_0$ or $\boldsymbol{F}_0$ must be related to the actual macroscopic variables $\boldsymbol{V}$ or $\boldsymbol{F}$. Some schemes rely on the simple choice $\boldsymbol{V}_0 = \boldsymbol{V}$ or $\boldsymbol{F}_0 = \boldsymbol{F}$, while other *effective field* schemes rely on $\boldsymbol{V}_0 \neq \boldsymbol{V}$ or $\boldsymbol{F}_0 \neq \boldsymbol{F}$. The effective fields $\boldsymbol{V}_0$ or $\boldsymbol{F}_0$ can be chosen in order to meet the velocity or force averaging rules (9) or (10) (average of velocity or force concentration tensors equal to $\boldsymbol{1}$).

In practice, the choices of the reference medium and the loading parameters are bundled in that of the homogenization scheme.

4.2. Dilute estimate or non-interacting approximation

In the dilute estimate, the RVE is assumed to comprise a matrix region Ω_m which can be represented with a permeability $\boldsymbol{k}_m$ and regions Ω_i of volume fractions $\varphi_i \ll 1$ constituted of disconnected inclusions. The inclusions are assumed sufficiently far apart such that for $i \neq m$ the region-wise averages $\overline{\boldsymbol{b}}^i$, $\overline{\boldsymbol{\kappa}}^i$ or $\overline{\boldsymbol{a}}^i$, $\overline{\boldsymbol{\rho}}^i$ of the concentration tensors (9) or (10) of problem P_{Stokes} can be approximated from their counterpart $\boldsymbol{B}_{i,m}$ or $\boldsymbol{A}_{i,m}$ (29) and the equivalent properties $\boldsymbol{k}_{i,m}$ or $\boldsymbol{r}_{i,m}$ (30) on distinct inhomogeneity problems with $\boldsymbol{V}_0 = \boldsymbol{V}$ or $\boldsymbol{F}_0 = \boldsymbol{F}$ and $\boldsymbol{k}_0 = \boldsymbol{k}_m$ (see fig. 3a), i.e.:

$$\begin{aligned}
&(i \neq m) \quad \overline{\boldsymbol{a}}^i \approx \boldsymbol{A}_{i,m} \quad \text{and} \quad \overline{\boldsymbol{\rho}}^i \approx \boldsymbol{r}_{i,m} \cdot \boldsymbol{A}_{i,m} \quad \Rightarrow \quad \overline{(\boldsymbol{\rho} - \boldsymbol{r}_m \cdot \boldsymbol{a})}^i \approx \boldsymbol{R}_{i,m} \quad \text{(velocity control)} \\
&(i \neq m) \quad \overline{\boldsymbol{b}}^i \approx \boldsymbol{B}_{i,m} \quad \text{and} \quad \overline{\boldsymbol{\kappa}}^i \approx \boldsymbol{k}_{i,m} \cdot \boldsymbol{B}_{i,m} \quad \Rightarrow \quad \overline{(\boldsymbol{\kappa} - \boldsymbol{k}_m \cdot \boldsymbol{b})}^i \approx \boldsymbol{K}_{i,m} \quad \text{(force control)}
\end{aligned} \tag{41}$$

where the last implications for the property contribution tensors $\boldsymbol{R}_{i,m}$ and $\boldsymbol{K}_{i,m}$ (36) result from relation (38). This *non-interacting approximation* leads to a *dilute estimate* of the homogenized permeability or resistance [5]:

$$\boldsymbol{r}_{\text{hom}} \approx \boldsymbol{r}_{\text{dil}} := \boldsymbol{r}_m + \overline{\boldsymbol{R}_{\cdot,m}} \quad \text{(velocity control)} \qquad ; \qquad \boldsymbol{k}_{\text{hom}} \approx \boldsymbol{k}_{\text{dil}} := \boldsymbol{k}_m + \overline{\boldsymbol{K}_{\cdot,m}} \quad \text{(force control)} \tag{42}$$

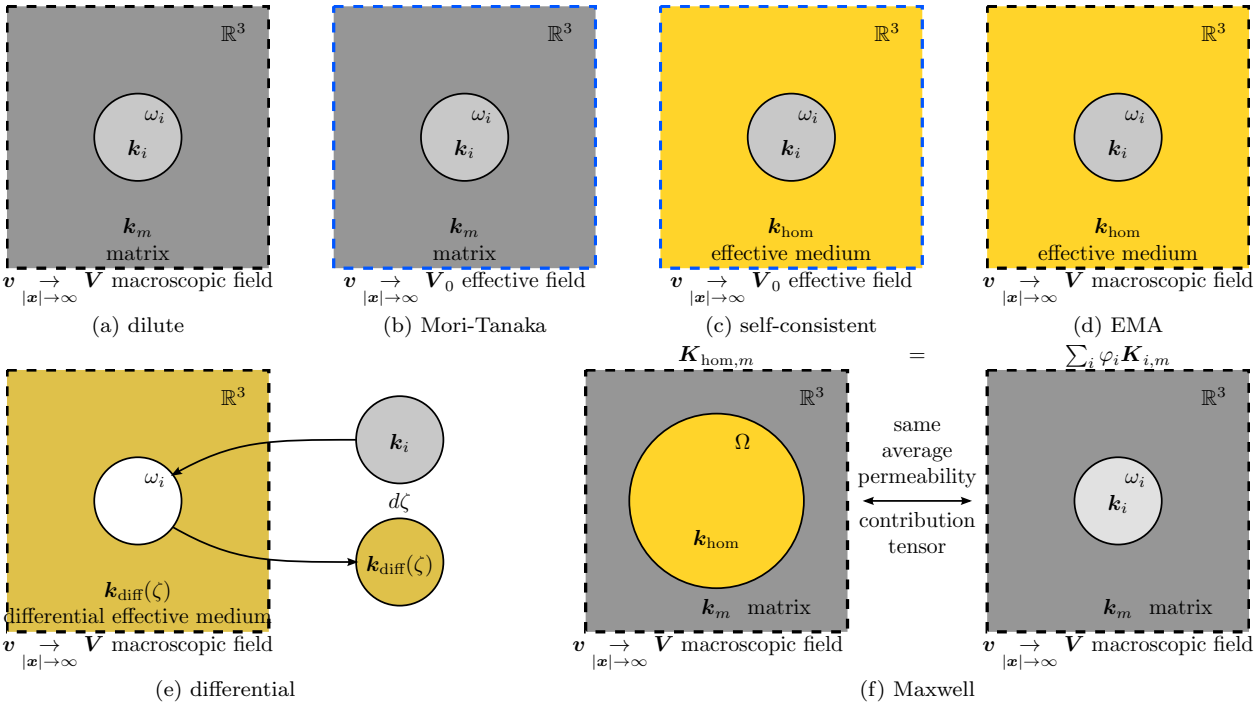

(a) dilute (b) Mori-Tanaka (c) self-consistent (d) EMA

(e) differential (f) Maxwell

Figure 3: Inhomogeneity problems used in homogenization schemes with their types of reference medium and remote load. For each region Ω_i of the RVE (except the matrix if any), an inhomogeneity ω_i is chosen as a representative pattern of Ω_i. The shape of the inhomogeneities ω_i may be arbitrary and their permeability $\boldsymbol{k}_i$ either homogeneous or heterogeneous. The schemes finally estimate the permeability by averaging relevant concentration tensors over all inhomogeneities.

where the overline with subscript $\cdot_{,m}$ denotes the volume average from inhomogeneity-based quantities with reference medium property $\boldsymbol{k}_m = \boldsymbol{r}_m^{-1}$, for example:

$$\overline{\boldsymbol{K}_{\cdot,m}} := \sum_i \varphi_i \boldsymbol{K}_{i,m} \tag{43}$$

For $i = m$ in eqs. (42), (43), the abusive but convenient notation $\boldsymbol{K}_{m,m} = \boldsymbol{R}_{m,m} = 0$ is used for the matrix region which is consistent that there is no property increment for an (in)homogeneity problem with $\boldsymbol{k} = \boldsymbol{k}_m$ everywhere.

The symmetry of $\boldsymbol{k}_{\text{dil}}$ and $\boldsymbol{r}_{\text{dil}}$ directly results from that of the property contribution tensors. Interestingly, (42) is reminiscent of the permeability increment (39) for the illustrative inhomogeneity in cell problem. The two estimates $\boldsymbol{r}_{\text{dil}}^{-1} \neq \boldsymbol{k}_{\text{dil}}$, but are equal at first order in $\varphi_i \ll 1$. For some specific applications, one of the estimate can provide a fair approximation beyond $\varphi_i \ll 1$ while the other would fail [5].

4.3. Mori-Tanaka-Benveniste estimate

The Mori-Tanaka estimate [8], as presented by Benveniste [9], is an effective field method which aims at alleviating shortcomings of the dilute estimate when the volume fraction of inhomogeneities is not infinitesimal.

The scheme applies to matrix-inclusion composites, with matrix permeability $\boldsymbol{k}_m$. For $i \neq m$, the region-wise averages of the velocity and body force $\overline{\boldsymbol{v}}^i$, $\overline{\boldsymbol{f}}^i$ of problem P_{Stokes} are approximated from their counterparts on distinct inhomogeneity problems with $\boldsymbol{V}_0 \neq \boldsymbol{V}$ or $\boldsymbol{F}_0 \neq \boldsymbol{F}$ (*effective fields*) and $\boldsymbol{k}_0 = \boldsymbol{k}_m$ (see fig. 3b). Additionally, the effective velocity $\boldsymbol{V}_0$ or force $\boldsymbol{F}_0$ is chosen as the average velocity or force over the matrix region Ω_m, i.e.:

$$\begin{aligned} \overline{\boldsymbol{v}}^i &\approx \boldsymbol{A}_{i,m} \cdot \boldsymbol{V}_0 \quad (i \neq m) \quad \text{and} \quad \overline{\boldsymbol{v}}^m \approx \boldsymbol{V}_0 \; (= \boldsymbol{A}_{m,m} \cdot \boldsymbol{V}_0) \quad \text{(velocity control)} \\ \overline{\boldsymbol{f}}^i &\approx \boldsymbol{B}_{i,m} \cdot \boldsymbol{F}_0 \quad (i \neq m) \quad \text{and} \quad \overline{\boldsymbol{f}}^m \approx \boldsymbol{F}_0 \; (= \boldsymbol{B}_{m,m} \cdot \boldsymbol{V}_0) \quad \text{(force control)} \end{aligned} \tag{44}$$

with the abusive but convenient notation $\boldsymbol{A}_{m,m} = \boldsymbol{B}_{m,m} = \boldsymbol{1}$ for the matrix region which is consistent with an (in)homogeneity problem with $\boldsymbol{k} = \boldsymbol{k}_m$ everywhere. The effective fields are determined from the averaging rule $\boldsymbol{V} = \overline{\boldsymbol{v}}^\Omega \approx \overline{\boldsymbol{A}_{\cdot,m}} \cdot \boldsymbol{V}_0$ (4) or $\boldsymbol{F} = \overline{\boldsymbol{f}}^\Omega \approx \overline{\boldsymbol{B}_{\cdot,m}} \cdot \boldsymbol{F}_0$ (see e.g. (9)) using the notation (43) for inhomogeneity-based average. Eventually, the concentration tensors are approximated for all regions by:

$$\begin{aligned} \overline{\boldsymbol{a}}^i &\approx \boldsymbol{A}_{i,m} \cdot \overline{\boldsymbol{A}_{\cdot,m}}^{-1} \quad \text{and} \quad \overline{\boldsymbol{\rho}}^i \approx \boldsymbol{r}_{i,m} \cdot \boldsymbol{A}_{i,m} \cdot \overline{\boldsymbol{A}_{\cdot,m}}^{-1} \quad \text{(velocity control)} \\ \overline{\boldsymbol{b}}^i &\approx \boldsymbol{B}_{i,m} \cdot \overline{\boldsymbol{B}_{\cdot,m}}^{-1} \quad \text{and} \quad \overline{\boldsymbol{\kappa}}^i \approx \boldsymbol{k}_{i,m} \cdot \boldsymbol{B}_{i,m} \cdot \overline{\boldsymbol{B}_{\cdot,m}}^{-1} \quad \text{(force control)} \end{aligned} \tag{45}$$

From (40), the Mori-Tanaka estimates to the homogenized permeability or resistance are:

$$\begin{aligned} \boldsymbol{r}_{\text{hom}} \approx \boldsymbol{r}_{\text{mt}} &:= \overline{\boldsymbol{r}_{\cdot,m} \cdot \boldsymbol{A}_{\cdot,m}} \cdot \overline{\boldsymbol{A}_{\cdot,m}}^{-1} = \boldsymbol{r}_m + \overline{\boldsymbol{R}_{\cdot,m}} \cdot \overline{\boldsymbol{A}_{\cdot,m}}^{-1} \quad \text{(velocity control)} \\ \boldsymbol{k}_{\text{hom}} \approx \boldsymbol{k}_{\text{mt}} &:= \overline{\boldsymbol{k}_{\cdot,m} \cdot \boldsymbol{B}_{\cdot,m}} \cdot \overline{\boldsymbol{B}_{\cdot,m}}^{-1} = \boldsymbol{k}_m + \overline{\boldsymbol{K}_{\cdot,m}} \cdot \overline{\boldsymbol{B}_{\cdot,m}}^{-1} \quad \text{(force control)} \end{aligned} \tag{46}$$

Provided $\boldsymbol{k}_m$ is neither vanishing nor infinite, $\boldsymbol{r}_{\text{mt}} = \boldsymbol{k}_{\text{mt}}^{-1}$ from (20) or (38). The Mori-Tanaka estimates $\boldsymbol{k}_{\text{mt}}$ and $\boldsymbol{r}_{\text{mt}}$ may be not symmetric.

4.4. Self-consistent estimate

The self-consistent estimate was developed for dielectric properties by Bruggeman [18] and subsequently in elasticity by [19–22].

In the self-consistent estimate, no phase has a specific role of matrix. The concentration rules are drawn from inhomogeneity problems (see fig. 3c) in which the reference material is an *effective medium*, i.e. the sought-for homogenized material, and the applied remote load is an *effective field* $\boldsymbol{V}_0$ or $\boldsymbol{F}_0$. Let $\boldsymbol{k}_{\text{sc}}$ the self-consistent estimate to $\boldsymbol{k}_{\text{hom}}$. The self-consistent estimate is build similarly to (45) but with a reference

medium of permeability $\boldsymbol{k}_0 = \boldsymbol{k}_{\rm sc}$ instead of a matrix. The concentration tensors are hence approximated by:

$$\begin{aligned} \overline{\boldsymbol{a}}^i &\approx \boldsymbol{A}_{i,\rm sc} \cdot \overline{\boldsymbol{A}_{\cdot,\rm sc}}^{-1} \quad \text{and} \quad \overline{\boldsymbol{\rho}}^i \approx \boldsymbol{r}_{i,\rm sc} \cdot \boldsymbol{A}_{i,\rm sc} \cdot \overline{\boldsymbol{A}_{\cdot,\rm sc}}^{-1} \quad \text{(velocity control)} \\ \overline{\boldsymbol{b}}^i &\approx \boldsymbol{B}_{i,\rm sc} \cdot \overline{\boldsymbol{B}_{\cdot,\rm sc}}^{-1} \quad \text{and} \quad \overline{\boldsymbol{\kappa}}^i \approx \boldsymbol{k}_{i,\rm sc} \cdot \boldsymbol{B}_{i,\rm sc} \cdot \overline{\boldsymbol{B}_{\cdot,\rm sc}}^{-1} \quad \text{(force control)} \end{aligned} \tag{47}$$

Replacing both $\boldsymbol{k}_m$ and $\boldsymbol{k}_{\rm mt}$ by $\boldsymbol{k}_{\rm sc}$ in (46), the self-consistent estimates to the homogenized permeability $\boldsymbol{k}_{\rm sc}$ and resistance $\boldsymbol{r}_{\rm sc}$ with $\boldsymbol{r}_{\rm sc} = \boldsymbol{k}_{\rm sc}^{-1}$ are equivalently defined by:

$$\begin{aligned} \boldsymbol{r}_{\rm hom} \approx \boldsymbol{r}_{\rm sc} &:= \overline{\boldsymbol{r}_{\cdot,\rm sc} \cdot \boldsymbol{A}_{\cdot,\rm sc}} \cdot \overline{\boldsymbol{A}_{\cdot,\rm sc}}^{-1} \quad \Leftrightarrow \quad \overline{\boldsymbol{R}_{\cdot,\rm sc}} = 0 \quad \text{(velocity control)} \\ \boldsymbol{k}_{\rm hom} \approx \boldsymbol{k}_{\rm sc} &:= \overline{\boldsymbol{k}_{\cdot,\rm sc} \cdot \boldsymbol{B}_{\cdot,\rm sc}} \cdot \overline{\boldsymbol{B}_{\cdot,\rm sc}}^{-1} \quad \Leftrightarrow \quad \overline{\boldsymbol{K}_{\cdot,\rm sc}} = 0 \quad \text{(force control)} \end{aligned} \tag{48}$$

The self-consistent estimate exhibits percolation thresholds: if one phase has a vanishing permeability, then the self-consistent estimate of the permeability will be zero for volume fractions of that phase above a critical value. In general, the value of the percolation threshold of the self-consistent scheme should not be considered as predictive of that of a specific microstructure. This threshold depends on the shapes of all inhomogeneities used to model the microstructure (see e.g. [89, Appendix B]).

4.5. Effective Medium Approximation

A distinction is here made between the terminologies "self-consistent" or "Effective Medium Approximation" (EMA). The term EMA may actually cover several methods in the literature: the self-consistent estimate of sec. 4.4 (which is an effective medium *and* effective field approximation), and the method described below, to which we simply refer as EMA herein. Indeed, this EMA is build from inhomogeneity problems with a reference medium of permeability $\boldsymbol{k}_0 = \boldsymbol{k}_{\rm ema}$ (effective medium), but with an applied remote load equal to the macroscopic velocity $\boldsymbol{V}$ or body force $\boldsymbol{F}$ (see figure 3d). As a result, the concentration tensors are approximated in EMA by:

$$\begin{aligned} \overline{\boldsymbol{a}}^i &\approx \boldsymbol{A}_{i,\rm ema} \quad \text{and} \quad \overline{\boldsymbol{\rho}}^i \approx \boldsymbol{r}_{i,\rm ema} \cdot \boldsymbol{A}_{i,\rm ema} \quad \text{(velocity control)} \\ \overline{\boldsymbol{b}}^i &\approx \boldsymbol{B}_{i,\rm ema} \quad \text{and} \quad \overline{\boldsymbol{\kappa}}^i \approx \boldsymbol{r}_{i,\rm ema} \cdot \boldsymbol{A}_{i,\rm ema} \quad \text{(force control)} \end{aligned} \tag{49}$$

As opposed to (47), the EMA estimates of $\overline{\boldsymbol{a}}^i$ or $\overline{\boldsymbol{b}}^i$ (49) may violate the averaging rules $\overline{\boldsymbol{a}}^\Omega = \boldsymbol{1}$ or $\overline{\boldsymbol{b}}^\Omega = \boldsymbol{1}$. The EMA estimates $\boldsymbol{k}_{\rm ema}$ and $\boldsymbol{r}_{\rm ema}$ to the homogenized permeability and resistance are build from a self-consistency condition which is an unscaled version of (48):

$$\boldsymbol{r}_{\rm hom} \approx \boldsymbol{r}_{\rm ema} := \overline{\boldsymbol{r}_{\cdot,\rm ema} \cdot \boldsymbol{A}_{\cdot,\rm ema}} \quad \text{(velocity control)} \qquad ; \qquad \boldsymbol{k}_{\rm hom} \approx \boldsymbol{k}_{\rm ema} := \overline{\boldsymbol{k}_{\cdot,\rm ema} \cdot \boldsymbol{B}_{\cdot,\rm ema}} \quad \text{(force control)} \tag{50}$$

Unlike the self-consistent estimate (48), the EMA estimates $\boldsymbol{k}_{\rm ema}$ and $\boldsymbol{r}_{\rm ema}$ may be not symmetric (see e.g. [90]).

The methods of [53–57] for Stokes to Darcy upscaling are EMA in the sense of (50) which feature a single composite inhomogeneity ω_1 with a solid (potentially porous) core, surrounded by a Stokes fluid envelop, itself embedded in an infinite effective medium. Denoting by $\boldsymbol{k}_{1,\rm ema}$ the equivalent permeability of the inhomogeneity as defined in (30), the EMA (50) is build from the self-consistency rule $\boldsymbol{k}_{\rm ema} = \boldsymbol{k}_{1,\rm ema} \cdot \boldsymbol{B}_{1,\rm ema}$, whereas the self-consistent scheme (48) directly requires the equality of the homogenized and equivalent permeabilities $\boldsymbol{k}_{\rm sc} = \boldsymbol{k}_{1,\rm sc}$ thanks to a proper scaling of the permeability. The two expressions differ since it turns out that $\boldsymbol{B}_{1,\rm ema} \neq \boldsymbol{1}$ in general.

4.6. Differential estimate or iterated dilute approximation

Differential estimates or differential effective medium have been first proposed by Roscoe [10] and Brinkman [11] for the effective viscosity of suspensions and latter in elasticity by [12–15]. The methodology was applied to Stokes to Darcy homogenization by Wilkinson [66] for a specific case of Brinkman inhomogeneity problem, under the denomination iterated dilute approximation.

The idea is to apply (42) by iteratively adding infinitesimal volume fractions of inhomogeneities to a reference medium defined as the homogenized property from the previous iteration (see fig. 3e). More precisely, the replacement process is described by a variable ζ such as at each step an incremental volume fraction $\mathrm{d}\zeta$ of the material homogenized from step ζ is replaced by inhomogeneities, starting from a reference material of permeability $\boldsymbol{k}_0 = \boldsymbol{k}_m$ at step $\zeta = 0$, where $\boldsymbol{k}_m$ is the permeability of the matrix region. The evolving volume fraction of each region Ω_i ($i \neq m$) is described by the current volume fraction ϕ_i varying from 0 at $\zeta = 0$ to φ_i at the end of the process. Similarly, the current overall volume fraction of inhomogeneities $\Phi = \sum_{i\neq m} \phi_i$ varies from 0 to $\sum_{i\neq m} \varphi_i$.

In the replacement, a volume fraction $\gamma_i \,\mathrm{d}\zeta$ of new inhomogeneities of each region i is introduced in the system, where γ_i is a filling rate which may depend on ζ, with $\sum_{i\neq m} \gamma_i = 1$. Due to overlaps with previously added inhomogeneities, the replacement removes a volume fraction $\phi_i \,\mathrm{d}\zeta$ of each region i, so that the net increase in volume fraction of this region is $\mathrm{d}\phi_i = (\gamma_i - \phi_i)\,\mathrm{d}\zeta$. The net increase of overall volume fraction of inhomogeneities is $\mathrm{d}\Phi = (1 - \Phi)\,\mathrm{d}\zeta$ which provides a one to one relationship between Φ and ζ:

$$\Phi = 1 - \exp(-\zeta) \tag{51}$$

Denoting by $\boldsymbol{k}_{\mathrm{dif}}(\Phi(\zeta))$ the permeability at iteration ζ, application of (42) gives the permeability increment

$$\boldsymbol{k}_{\mathrm{dif}}(\Phi + \mathrm{d}\Phi) - \boldsymbol{k}_{\mathrm{dif}}(\Phi) = \sum_{i\neq m} \gamma_i \,\mathrm{d}\zeta\, \boldsymbol{K}_{i,\mathrm{dif}(\Phi)} \quad \Leftrightarrow \quad \frac{\mathrm{d}\boldsymbol{k}_{\mathrm{dif}}}{\mathrm{d}\Phi} = \frac{1}{1-\Phi} \sum_{i\neq m} \gamma_i \boldsymbol{K}_{i,\mathrm{dif}(\Phi)} \tag{52}$$

Eq. (52) with the initial condition $\boldsymbol{k}_{\mathrm{dif}}(\Phi = 0) = \boldsymbol{k}_m$ defines the differential estimate of the permeability by a tensorial differential equation, which degenerates to a scalar one in the case of overall isotropy.

The differential estimate does not introduce a percolation of the region $i \neq m$, regardless of their volume fractions (except in the degenerate situation $\Phi = 1$), unless inhomogeneities of the matrix $\boldsymbol{k}_m$ are artificially introduced (see [15]). Reciprocal definition of (52) in terms of resistance leads to the exact inverse of $\boldsymbol{k}_{\mathrm{dif}}$ [14], except if $\boldsymbol{k}_0$ is either vanishing or infinite. The distinction between ζ and Φ via $\mathrm{d}\Phi = (1 - \Phi)\,\mathrm{d}\zeta$ and (51) allows to retrieve the self-consistent estimate (48) in the limit $\Phi \to 1$ with the proportional filling rule introduced below (see [15]).

The relative rates of filling with different regions, which can be described by a path in the space of the $\{\phi_i\}$, modifies the output of the differential estimate [15]. Some simple choices are:

(a) *proportional filling*, i.e. $\alpha_i = \varphi_i / \sum_{j\neq m} \varphi_j$ [5, 13, 14].
(b) *sequential filling*, say only region $i = 1$ first, then only region $i = 2$, and so on [66]. As the replacement by a region i removes inhomogeneities from regions $j \leq i$, it is necessary to introduce excess of the first regions to reach the target final volume fractions.

Choice (b) leads to non-monotonous evolution of the current volume fraction which was excluded from possibilities investigated in [15] as non-physical. Nonetheless, choice (b) has been used by Wilkinson [66] to estimate the permeability of materials made of impervious solid spherical grains with a particle size distribution.

4.7. Maxwell estimate

We here follow the reformulation of the Maxwell estimate [16] in terms of property contribution tensors by [5, 17]. The Maxwell estimate is suited to matrix-inclusion composites, and the matrix permeability $\boldsymbol{k}_m$ is taken as the reference permeability in all inhomogeneity problems below. The homogenized permeability $\boldsymbol{k}_{\mathrm{hom}}$ of the RVE Ω is estimated by $\boldsymbol{k}_{\mathrm{Max}}$ chosen such that the permeability contribution tensor (36) of an equivalent inhomogeneity of uniform permeability $\boldsymbol{k}_{\mathrm{Max}}$ is equal to the volume average of the permeability contribution tensors of all inhomogeneities ω_i (see fig. 3f):

$$\boldsymbol{K}_{\mathrm{Max},m}(\Omega) = \overline{\boldsymbol{K}_{\cdot,m}} \tag{53}$$

In the left-hand side of (53), the equivalent inhomogeneity replaces the whole domain Ω. The Maxwell estimate thus introduces a dependence of the homogenized permeability on the shape of the RVE and, apart

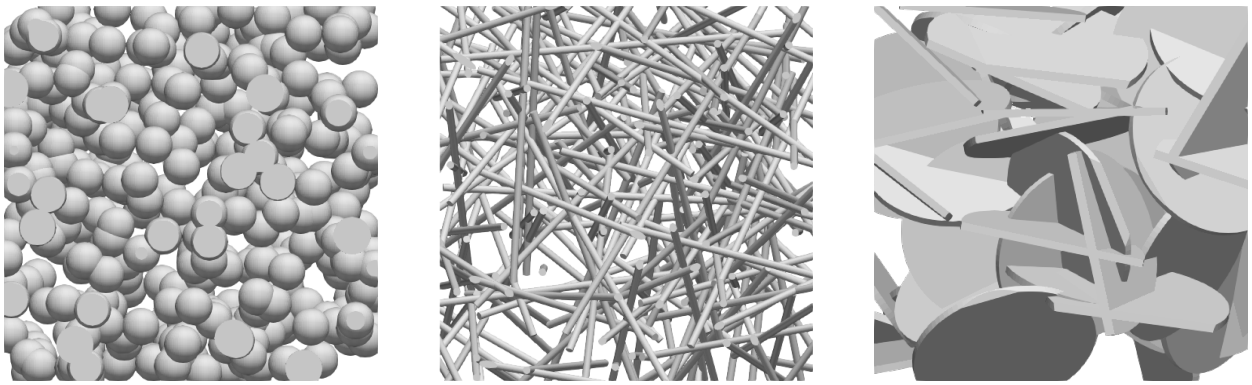

(a) spheres (b) elongated cylinders (c) flat cylinders

Figure 4: Examples of Boolean models of spheres and elongated or flat cylinders

from the asymptotic case discussed below, on its size. This is a major issue concerning its interpretation and may lead to inconsistencies in some situations, which can be mitigated by a careful analysis [5] in the conduction or elasticity settings.

The dependence of $\boldsymbol{k}_{\mathrm{Max}}$ on the size L_Ω of the RVE can be alleviated since L_Ω is much larger than the characteristic size ℓ_ω of the inhomogeneities. Apart from the situation where the reference medium is a Stokes fluid ($\boldsymbol{k}_m \to \infty$), ℓ_ω is usually much larger the characteristic size ℓ_m given by $\boldsymbol{k}_m$ (e.g. $\ell_m = \sqrt{k}_m$ for $\boldsymbol{k}_m = k_m \mathbf{1}$). Hence, in the Brinkman inhomogeneity problem involving the inhomogeneity of permeability $\boldsymbol{k}_{\mathrm{Max}}$ and size L_Ω, the effects of Brinkman layer – which occur in a layer of thickness $\mathcal{O}(\ell_m)$ – are negligible. The laplacian of $\boldsymbol{v}$ is much smaller than $\boldsymbol{k}_m \cdot \boldsymbol{v}$ and Darcy equation are asymptotically retrieved (see e.g. figure A.12 as $R/\ell_m \to \infty$). In that case, provided that the shape chosen to represent the RVE Ω is ellipsoidal, one may approximate the permeability contribution tensor $\boldsymbol{K}_{\mathrm{Max},m}(\Omega)$ of the homogenized RVE by its closed form expression from the Darcy inhomogeneity problem, namely:

$$\lim_{L_\Omega/\ell_m \to \infty} \boldsymbol{K}_{\mathrm{Max},m}(\Omega) = \left[(\boldsymbol{k}_{\mathrm{Max}} - \boldsymbol{k}_m)^{-1} + \boldsymbol{P}_m^\Omega \right]^{-1} \tag{54}$$

where $\boldsymbol{P}_m^\Omega$ is the Hill tensor of the ellipsoidal shape Ω in the reference Darcy medium of permeability $\boldsymbol{k}_m$, which does not depend on the absolute size of Ω and is known explicitly [36].

Clearly, this asymptotic situation does not apply to Stokes to Darcy homogenization if the matrix is the Newtonian fluid, i.e. $\boldsymbol{r}_m = 0$ and thus $\ell_m \to \infty$. In that case, solution of Stokes flow past a Brinkman inhomogeneity introduces a strong dependence on the inhomogeneity size, and use of the Maxwell scheme is discouraged.

5. Assessment of homogenization schemes on full field simulations

The different homogenization schemes presented in section 4 are now compared to a wide range of microstructure types to illustrate their flexibility, show their range of validity and highlight some pitfalls.

5.1. Worked-out example: granular porous media with impermeable grains

Let us work out the estimates presented in section 4 in the case where the porous medium comprises a solid phase made out of impermeable grains (phase s) and a complementary Stokes fluid phase (phase p). The porosity is denoted by φ. The homogenized permeabilities will be compared in figure 5 to the following model granular media:

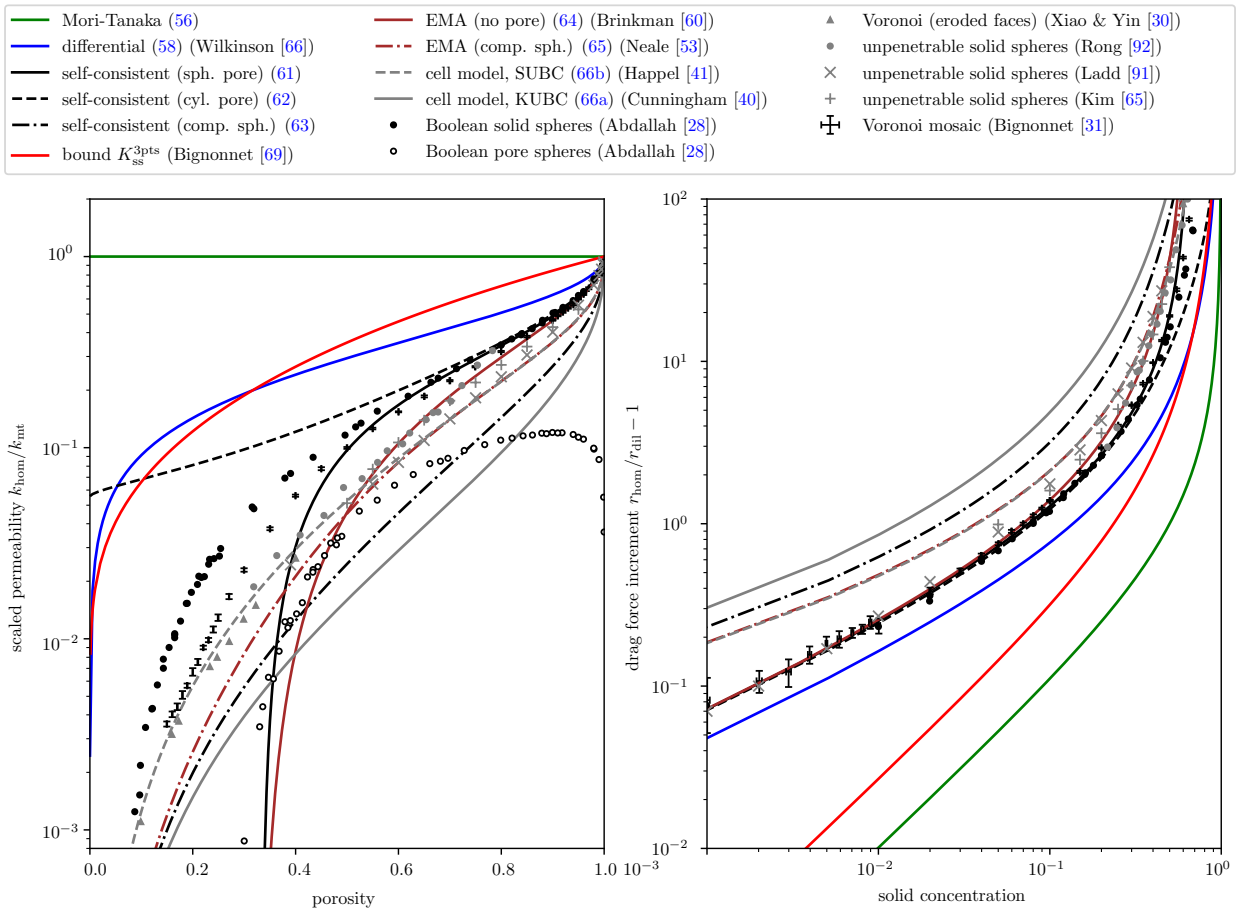

Figure 5: Permeability of a granular porous medium with spherical grains of equal radius R or Voronoi cells, scaled by $k_{mt} = \frac{2R^2\varphi}{9(1-\varphi)}$ (left) or $r_{dil} = \frac{9(1-\varphi)}{2R^2}$ (right), as a function of the porosity φ.

(a) Boolean model of spheres (fig. 4a), with equisized spheres of radius R that have centers randomly positioned according to a random Poisson process and may overlap. Simulation results are available from [28].

(b) Unpenetrable spheres, with randomly positioned but non-overlapping equisized spheres. Reference results are taken from fluid dynamics models [65, 91] and simulations [92].

(c) Voronoi mosaic, with Voronoi cells randomly labeled as solid or pore. Simulations results are from [31]. Permeability is scaled by an equivalent grain radius R computed so as to meet the two previous sphere models in the dilute limit $\varphi \to 1$.

(d) Voronoi cells with eroded faces, obtained by erosion of cells in a Voronoi tessellation from faces, leaving disconnected solid polyhedrons separated by planar pores with constant opening thickness t (i.e. t is the distance between the faces of two neighbouring solid polyhedrons) [30]. Permeability is scaled by an equivalent grain radius R computed by matching the porosity of a composite sphere model with a solid core of radius R and a fluid shell of radius $R + t/2$.

Dilute scheme. Selecting the Stokes fluid as the matrix ($\boldsymbol{r}_0 = \boldsymbol{r}_m \to 0$), combination of (42) and (A.3b) with $\alpha_0 \to 0$ yields the dilute estimate of the resistance of a bed of spheres with volume fraction $1 - \varphi \ll 1$:

$$r_{dil} = (1-\varphi)\frac{9}{2R^2} \tag{55}$$

Mori-Tanaka scheme. Since the velocity and hence $\boldsymbol{A}_{s,p}$ vanish in the solid phase, while the drag force hence $\boldsymbol{r}_p \cdot \boldsymbol{A}_{p,p}$ vanish in the pore phase, the Mori-Tanaka estimate (46) of the resistance here is simply:

$$r_{\rm mt} = \frac{1-\varphi}{\varphi}\frac{9}{2R^2} \tag{56}$$

which corrects (55) to yield $k_{\rm mt} \to 0$ as the porosity $\varphi \to 0$, but largely overestimates the permeability for all comparison granular models in fig. 5.

Differential scheme. The differential equation of the differential estimate (52) written in terms of resistance here requires the concentration tensor (A.3b) with α_0 set to $\alpha_{\rm diff} = R\sqrt{r_{\rm diff}}$:

$$-\frac{{\rm d}r_{\rm dif}}{{\rm d}\varphi} = \frac{1}{\varphi}R_{s,{\rm dif}} = \frac{1}{\varphi}\frac{3\left(3+3\alpha_{\rm diff}+\alpha_{\rm diff}^2\right)}{2R^2} \tag{57}$$

The latter can be integrated analytically [66] to give the implicit definition of $r_{\rm diff}$:

$$-\tfrac{3}{2}\ln\varphi = \ln(1+\alpha_{\rm diff}+\alpha_{\rm diff}^2/3) - 2\sqrt{3}\left[\arctan\left(\tfrac{2}{\sqrt{3}}\alpha_{\rm diff}+\sqrt{3}\right) - \tfrac{\pi}{3}\right] \tag{58}$$

The differential estimate improves on the Mori-Tanaka one for the models in fig. 5, yet still overestimates the permeability and violates at low porosities the three point correlation upper bound K_{ss}^{3pts} derived in [69] for the Boolean model of spheres.

Self-consistent scheme. The self-consistent estimate requires a description of all phases by relevant Brinkman inhomogeneity problems. If the solid phase is obviously represented by a spherical inhomogeneity of radius $R_s = R$ and uses (A.3b) as previously, an inhomogeneity shape has to be chosen for the pore phase.

Spherical pores. Let us start with the simplest choice, namely spherical pores of equal radius R_p. Then the velocity concentration in pores is given by (A.3a) and the self-consistent estimate (48) of the permeability is the solution to:

$$(1-\varphi)\,\frac{3\left(3+3\alpha_{s,{\rm sc}}+\alpha_{s,{\rm sc}}^2\right)}{2R_s^2} \;-\; \varphi\, r_{\rm sc}\, 3\frac{15+15\alpha_{p,{\rm sc}}+6\alpha_{p,{\rm sc}}^2+\alpha_{p,{\rm sc}}^3}{45+45\alpha_{p,{\rm sc}}+6\alpha_{p,{\rm sc}}^2+\alpha_{p,{\rm sc}}^3} = 0 \tag{59}$$

with $\alpha_{s,{\rm sc}} = R_s\sqrt{r_{\rm sc}}$ for the grains and $\alpha_{p,{\rm sc}} = R_p\sqrt{r_{\rm sc}}$ for the pores.

To proceed, we need a rule to set the spherical pore radius R_p as a function of the spherical solid grain radius R_s. The rule is defined by requesting that the specific surface area of the solid–fluid interface seen from a pore inhomogeneity is the same as the one seen from a solid grain inhomogeneity. For both inhomogeneities, the reference medium is the homogenized medium so that it is reasonable to assume that in average over all pore or solid inhomogeneities, a fraction φ (resp. $1-\varphi$) of the inhomogeneity–reference medium interface is an inhomogeneity–pore (resp. inhomogeneity–solid) interface. Let us denote s_i the specific surface area of an inhomogeneity i ($i = p$, pore or $i = s$, solid). From the point of view of the pore inhomogeneities, the specific surface area between pores and solid is: specific surface area of the inhomogeneity (s_p) times portion of that area in contact with solid ($1-\varphi$) times volume proportion of such inhomogeneity in the material (p), hence $s_p \times (1-\varphi) \times \varphi$, while it is $s_s \times \varphi \times (1-\varphi)$ from the solid inhomogeneity point of view. The equality of these two specific surface areas is fulfilled if:

$$s_p = s_s \tag{60}$$

Since we here have spherical shapes for all phases, (60) requires $R_s = R_p$ and (59) simplifies to:

$$\frac{1-\varphi}{\varphi} = \frac{2\alpha_{\rm sc}^2(15+15\alpha_{\rm sc}+6\alpha_{\rm sc}^2+\alpha_{\rm sc}^3)}{(3+3\alpha_{\rm sc}+\alpha_{\rm sc}^2)(45+45\alpha_{\rm sc}+6\alpha_{\rm sc}^2+\alpha_{\rm sc}^3)} \quad \text{with} \quad \alpha_{\rm sc} = R\sqrt{r_{\rm sc}} \tag{61}$$

Despite its relative simplicity, the self-consistent estimate defined by (61) provides an almost perfect agreement with simulation data on the Boolean model of spheres and the Voronoi mosaic for porosities above

50%. It reproduces exactly the non-analytical behavior of the drag force due to interactions between multiple spheres, with the leading term $r_{\rm hom}/r_{\rm dil} = 1 + \frac{3}{\sqrt{2}}\sqrt{1-\varphi} + o(\sqrt{1-\varphi})$ [63–65] (see fig. 5, right).

As in Darcy to Darcy or conduction homogenization, the self-consistent model with spherical shapes (61) features a porosity percolation threshold of $\frac{1}{3}$. It is obviously inappropriate to describe the permeability of the Boolean model of spheres which has a porosity percolation threshold $\varphi_c \approx 3\%$, because the spherical shape used for pores is not an appropriate representation of the actual concave shaped pores. Interestingly, the complementary "swiss-cheese" model with Boolean spherical pores in an impermeable matrix has a threshold $\varphi_c \approx 29\%$ ([28], empty dots in fig. 5) which is closer to $\frac{1}{3}$. In general, the value of the percolation threshold of the self-consistent scheme should not be considered as predictive of that of a specific microstructure.

Cylindrical pores. To go beyond the spherical pore assumption, the present framework theoretically allows the use of arbitrary shapes of inhomogeneities, for example concave shaped pores as used in [93–95] for elasticity and conduction homogenization. Since solutions to Brinkman inhomogeneity problems with concave pores are yet not available, use of such pores is not possible to day. However, let us illustrate the effect of the pore shape on the output of the self-consistent scheme by representing pores via the Brinkman inhomogeneity problem of an infinitely elongated cylindrical pore of radius R_p. The concentration tensor for a cylindrical pore is now given in (A.9a) and involves modified Bessel functions as well as a unit vector $\boldsymbol{n}$ which indicates the orientation of the cylinder axis. The cylinders are assumed to follow an isotropic distribution of orientations, so that upon summation over all pores only the orientation averages of the tensors $\mathbf{1}_n = \boldsymbol{n}\otimes\boldsymbol{n}$ and $\mathbf{1}_t = (\mathbf{1} - \boldsymbol{n}\otimes\boldsymbol{n})$ are required, and equal to $\frac{1}{3}\mathbf{1}$ and $\frac{2}{3}\mathbf{1}$ respectively. The self-consistent estimate (48) of the permeability is now the solution to:

$$\begin{aligned}&(1-\varphi)\,\frac{3\left(3+3\alpha_{s,\rm sc}+\alpha_{s,\rm sc}^2\right)}{2R_s^2}\\ &-\varphi\, r_{\rm sc}\left(\tfrac{1}{3}\frac{8+\alpha_{p,\rm sc}^2+4\alpha_{p,\rm sc}K_1^0(\alpha_{p,\rm sc})}{8}+\tfrac{2}{3}2\frac{8+\alpha_{p,\rm sc}^2+4\alpha_{p,\rm sc}K_1^0(\alpha_{p,\rm sc})}{16+\alpha_{p,\rm sc}^2+4\alpha_{p,\rm sc}K_1^0(\alpha_{p,\rm sc})}\right)=0\end{aligned} \tag{62}$$

where $\alpha_{s,\rm sc} = R_s\sqrt{r_{\rm sc}}$ and $\alpha_{p,\rm sc} = R_p\sqrt{r_{\rm sc}}$. To link the cylindrical pore radius R_p to the solid grain one R_s, we invoke again the specific surface area requirement (60). For a cylinder $s_p = 2/R_p$ while $s_s = 3/R_s$ for the sphere, hence $R_p = \frac{2}{3}R_s$ is chosen. By doing so, the two self-consistent estimates (61) and (62) have exactly the same behavior in the dilute regime $\varphi \to 1$, as seen in the right of figure 5. If a different value of R_p were selected, this correspondence would break down.

Interestingly, use of cylindrical pores ensures percolation of the self-consistent estimate at all porosities. Intermediate values of porosity percolation threshold $0 < \varphi_c < \frac{1}{3}$ are expected for spheroidal pore shapes, as well as a better agreement with comparison granular models in fig. 5 at low porosity. The solution to the spheroidal Brinkman inhomogeneity is unfortunately known only for an axial loading [96].

Composite spherical inhomogeneity. Another way to describe the pore space is to resort to a composite inhomogeneity. A single type inhomogeneity ω_1 with volume fraction 1 is used. The composite spherical inhomogeneity ω_1 has an impermeable spherical core of radius R surrounded by a concentric spherical Stokes fluid shell of radius $R/\sqrt[3]{1-\varphi}$, itself embedded in a Brinkman medium of permeability equal to the sought-for homogenized permeability. The concentration tensors are given in (A.4). The self-consistent equation (48) collapses to:

$$\boldsymbol{r}_{\rm sc} = \boldsymbol{r}_{1,\rm sc} \tag{63}$$

where $\boldsymbol{r}_{1,\rm sc}$ is the equivalent resistance of the composite inhomogeneity defined according to (30) and given by replacing α_0 by $R\sqrt{r_{\rm sc}}$ in (A.5). The composite sphere self-consistent estimate underestimates the permeability w.r.t. comparison granular models in fig. 5 but produces the correct order of magnitude on the whole porosity range. As for other cell models [97], the non-analytic corrective term in the average drag force is incorrectly reproduced, with a behavior in $\sqrt[3]{1-\varphi}$ instead of $\sqrt{1-\varphi}$.

Brinkman's original self-consistent model. Eq. (61) is not to be confused with the original self-consistent method or effective medium approximation of Brinkman [60]:

$$r_{\rm brinkman} = (1-\varphi)\,\frac{3\left(3+3\alpha_{\rm brinkman}+\alpha_{\rm brinkman}^2\right)}{2R^2} \quad \text{with} \quad \alpha_{\rm brinkman} = R\sqrt{r_{\rm brinkman}} \tag{64}$$

in which the role of the pore phase is obliterated. Eqs. (61) and (64) both percolate at $\varphi = \frac{1}{3}$ and provide the same leading term as $\varphi \to 1$, but in the range $\varphi > 0.5$ eq. (61) agrees with the Boolean model of spheres while eq. (64) agrees with the model of unpenetrable spheres.

Effective medium approximation. As detailed in sec. 4.5, the self-consistent estimate with a composite sphere ω_1 (63) is not to be confused with the effective medium approximation (EMA) used by [53, 54]. The implicit equation defining the EMA estimate $\boldsymbol{r}_{\text{ema}}$ to the resistance is:

$$\boldsymbol{r}_{\text{ema}} = \boldsymbol{r}_{1,\text{ema}} \cdot \boldsymbol{A}_{1,\text{ema}} \tag{65}$$

The EMA (65) lies slightly above (63) and slightly below comparison granular models in fig. 5.

Cell models. In cell models, a composite cell Ω_0 identical to the composite inhomogeneity used in (63) or (65) is considered with boundary conditions applied directly on the boundary of the cell. Several choices of boundary conditions have been investigated [41, 45, 49], we here only present the KUBC and SUBC (see (13)) which gives respectively minimum and maximum values of the apparent permeability (21) for these types of cell models:

$$k_{\text{app}}^{\text{KUBC}} = \frac{(1-\eta)^3(4+7\eta+4\eta^2)}{18\eta^3(1+\eta+\eta^2+\eta^3+\eta^4)} R^2 \tag{66a}$$

$$k_{\text{app}}^{\text{SUBC}} = \frac{(1-\eta)^3(1+\eta)(2+\eta+2\eta^2)}{3\eta^3(3+2\eta^5)} R^2 \tag{66b}$$

with $\eta = \sqrt[3]{1-\varphi}$. The SUBC estimate (66b) coincides with the zero shear stress BC of Happel [41] in that case, and provides a good agreement with the unpenetrable sphere model and the eroded face Voronoi model in fig. 5. Estimates (66) bound the composite self-consistent estimate (63) and EMA (65).

Discussion. Figure 5 illustrates discrepancies with reference results that can arise from the use of the various homogenization schemes. For such materials, schemes based on a clear fluid reference medium like the dilute (55) and Mori-Tanaka (56) schemes are inappropriate: they capture only the leading asymptotic term as $\varphi \to 1$ and fail to reproduce the first corrective term $\frac{3}{\sqrt{2}}\sqrt{1-\varphi}$ on the drag force increment. This result is expected since the use of a clear fluid reference medium cannot reproduce the average field far from a grain. The differential scheme (58) provides a partial but insufficient correction. Conversely, schemes relying on an effective medium such as the self-consistent scheme (61),(62) reproduce the first corrective term $\frac{3}{\sqrt{2}}\sqrt{1-\varphi}$ – which confirms the interest in using Brinkman's law in the inhomogeneity problems –, unless the porosity is represented as a shell around a spherical grain using a composite sphere (63), (65). As for cell models (66), the composite sphere indeed introduces a $\sqrt[3]{1-\varphi}$ corrective term improper at low solid concentration due to a placement of porosity which is too regular and leads to an underestimation of the permeability. A major result of this work is that porosity can be represented differently than by a composite sphere using homogenization schemes. Under requirement (60), the two self-consistent estimates with spherical (61) or cylindrical (62) pores illustrate that the shape of the inhomogeneities used to represent pores becomes increasingly important as the porosity decreases. As compared to the Voronoi mosaic or Boolean solid sphere models, a good agreement is provided by (61),(62) for solid concentrations as high as 50%. But for lower porosities, a representation of pores by spheres (61) underestimates (resp. cylinders (62) overestimates) the connectivity of the pore phase: more appropriate pore shapes (spheroidal, concave, ...) should be used to achieve a realistic porosity percolation threshold.

5.2. Fibrous porous media with impermeable fibers

A detailed study of the permeability of fibrous media can be found in Jackson and James [98], including a large experimental database and a review of permeability homogenization models such as periodic arrangements of fibres or cylindrical cell models. The homogenized permeabilities will here be compared in figure 5 to the following actual or model fibrous media:

(a) Experimental results gathered in [98, 99] on a variety of fibrous media.
(b) Boolean model of cylinders [29] with isotropic distribution of orientations (see fig. 4b).
(c) Voronoi fibrous model [30], which is obtained by dilation of the edges of the cells of Voronoi tessellations.

Dilute, Mori-Tanaka and differential schemes. Because of Stokes' paradox, the inhomogeneity problem of an isolated solid cylinder in an infinite Stokes fluid cannot be used, hence the dilute, Mori-Tanaka and differential estimates cannot be defined here. This meets the above discussion in sec. 5.1 that clear fluid is not an appropriate reference medium as it fails to represent the average behavior in the far field.

Self-consistent scheme. The self-consistent estimate (48) is built from cylindrical impermeable inhomogeneities (A.9b) of radius $R_s = R$ together with a spherical (A.3a) or cylindrical (A.9a) Stokes inhomogeneity of radius R_p with $R_p = \frac{3}{2}R_s$ for the spherical pore and $R_p = R_s$ for the cylindrical pore from (60). The implicit equation for spherical (67a) or cylindrical (67b) pores are, with $\alpha_{i,\mathrm{sc}} = R_i\sqrt{r_{\mathrm{sc}}}$:

$$(1-\varphi)\frac{\big(2+\alpha_{s,\mathrm{sc}}K_1^0(\alpha_{s,\mathrm{sc}})\big)}{\alpha_{s,\mathrm{sc}}K_1^0(\alpha_{s,\mathrm{sc}})}\frac{5}{3} - 3\varphi\frac{15+15\alpha_{p,\mathrm{sc}}+6\alpha_{p,\mathrm{sc}}^2+\alpha_{p,\mathrm{sc}}^3}{45+45\alpha_{p,\mathrm{sc}}+6\alpha_{p,\mathrm{sc}}^2+\alpha_{p,\mathrm{sc}}^3} = 0 \tag{67a}$$

$$(1-\varphi)\frac{\big(2+\alpha_{s,\mathrm{sc}}K_1^0(\alpha_{s,\mathrm{sc}})\big)}{\alpha_{s,\mathrm{sc}}K_1^0(\alpha_{s,\mathrm{sc}})}\frac{5}{3} - \frac{\varphi}{3}\left(\frac{8+\alpha_{p,\mathrm{sc}}^2+4\alpha_{p,\mathrm{sc}}K_1^0(\alpha_{p,\mathrm{sc}})}{8} + 4\frac{8+\alpha_{p,\mathrm{sc}}^2+4\alpha_{p,\mathrm{sc}}K_1^0(\alpha_{p,\mathrm{sc}})}{16+\alpha_{p,\mathrm{sc}}^2+4\alpha_{p,\mathrm{sc}}K_1^0(\alpha_{p,\mathrm{sc}})}\right) = 0 \tag{67b}$$

The self-consistent estimates (67a) and (67b) are in close agreement with the Boolean cylinders [29] or Voronoi fibrous [30] models for $\varphi > 0.5$. The use of spherical pores in (67a) leads to a percolation threshold around 35%, while cylindrical pores always percolate. Neither spherical nor cylindrical pores are representative of the actual pore shapes, which explains the discrepancy with numerical results at lower porosity.

Effective medium approximation. EMA have been derived by embedding the composite cylinders either in an effective Darcy [100] or Brinkman [54] reference medium with remote boundary conditions. The results of [54], as well as the self-consistent estimate with a composite cylindrical inhomogeneity (48), are not reported in figure 6 as they both lie within the bounds (68). The transposition of Brinkman's model for spheres [60] to cylinders is treated by [101] and lies below the self-consistent model with spherical pores and cylindrical solids.

Cell models. Cylindrical cell models [42, 45, 46, 51] feature a composite cylinder made of a solid core of radius R and a Stokes fluid envelope of radius R/η, where η is usually set to match the overall porosity φ as $\eta = \sqrt{1-\varphi}$. For a single cylinder of axis along the unit vector $\boldsymbol{n}$, apparent permeabilities (21) with KUBC or SUBC – which here coincides with the no shear stress BC of [42] – are [45, Appendix A]:

$$\boldsymbol{k}_{\mathrm{app}}^{\mathrm{KUBC}} = -\frac{R^2}{\eta^2}\left(\ln\eta + \frac{1-\eta^2}{1+\eta^2}\right)\left[\frac{1}{2}\mathbf{1}_n + \frac{1}{4}\mathbf{1}_t\right] \tag{68a}$$

$$\boldsymbol{k}_{\mathrm{app}}^{\mathrm{SUBC}} = -\frac{R^2}{\eta^2}\left[\left(\ln\eta + \frac{(1-\eta^2)(3-\eta^2)}{4}\right)\frac{1}{2}\mathbf{1}_n + \left(\ln\eta + \frac{1-\eta^4}{2(1+\eta^4)}\right)\frac{1}{4}\mathbf{1}_t\right] \tag{68b}$$

To deal with an isotropic distribution of orientations of the fibers, the orientation averages of (68) are taken in figure 6. This amounts to replace $\mathbf{1}_n$ and $\mathbf{1}_t$ by $\frac{1}{3}\mathbf{1}$ and $\frac{2}{3}\mathbf{1}$ respectively. The cell models (68) encompass most of the experimental results gathered in [98, 99], but tend to underestimate the simulation results on the Boolean model of cylinders [29] and the Voronoi fibrous model [30], similarly to their counterparts in sec. 5.1.

5.3. Materials with tubular or crack-like pores

The homogenized permeabilities are compared in figure 7 to numerical simulations on the following model porous media:

(a) Boolean model of elongated (resp. flat) cylinders of radius R (resp. thickness $2R$) [29] with isotropic distribution of orientations (see fig. 4b or 4c)

(b) Voronoi tubular (resp. granular) model with tube radii R (resp. intergranular distance $2R$) [30], which is obtained by erosion from the edges (resp. faces) of the cells of Voronoi tessellations

As opposed to section 5.2, flow now occurs only *inside* the cylinders or eroded parts.

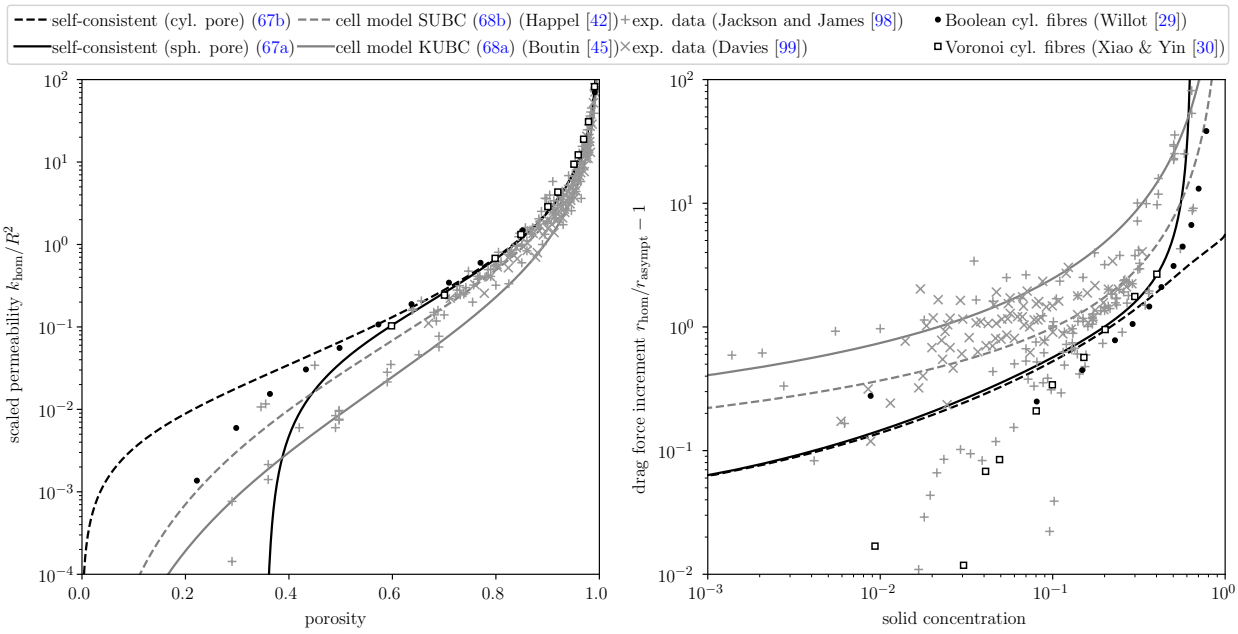

Figure 6: Permeability of a fibrous porous medium with cylindrical fibres of equal radius R, scaled by $r_{\rm asympt} = \frac{6(1-\varphi)}{-\ln(1-\varphi)R^2}$, as a function of the porosity φ.

Mori-Tanaka scheme. The matrix is the impermeable solid, while the inhomogeneity problems feature Stokes fluid inhomogeneities, either cylindrical or planar. Flow is possible in the axial (resp. transverse) direction of the cylindrical (resp. planar) pore inhomogeneities since they are unbounded: these problems actually correspond to Poiseuille's flows. The concentration tensors for the cylinder of axis $\boldsymbol{n}$, radius R is $\lim_{k_p\to\infty} \boldsymbol{k}_p \cdot \boldsymbol{B}_{p,s} = \frac{R^2}{8}\mathbf{1}_n$ and of the planar pore of normal $\boldsymbol{n}$, thickness $2R$ is $\lim_{k_p\to\infty} \boldsymbol{k}_p \cdot \boldsymbol{B}_{p,s} = \frac{R^2}{3}\mathbf{1}_t$. The Mori-Tanaka estimate (46) is:

$$k_{\rm mt} = \frac{R^2}{24}\frac{\varphi}{1-\varphi} \quad \text{(tubular pores)} \quad ; \quad k_{\rm mt} = \frac{2R^2}{9}\frac{\varphi}{1-\varphi} \quad \text{(planar pores)} \tag{69}$$

Differential scheme. Starting from the solid as the background medium ($k_{\rm dif}(\varphi=0)=0$), the differential estimate (52) is built by iteratively adding cylindrical or planar pores. Their permeability contribution tensors (36) are readily obtained from (A.9a) or (A.12a) and (20). The ordinary differential equations defining $k_{\rm dif}$ with $\alpha_{\rm dif} = R/\sqrt{k_{\rm dif}}$ are:

$$\frac{{\rm d}k_{\rm dif}}{{\rm d}\varphi} = \frac{k_{\rm dif}}{3(1-\varphi)}\left[\frac{8+\alpha_{\rm dif}^2+4\alpha_{\rm dif}K_1^0(\alpha_{\rm dif})}{8} + 4\frac{8+\alpha_{\rm dif}^2+4\alpha_{\rm dif}K_1^0(\alpha_{\rm dif})}{16+\alpha_{\rm dif}^2+4\alpha_{\rm dif}K_1^0(\alpha_{\rm dif})}\right] \quad \text{(tubular pores)} \tag{70a}$$

$$\frac{{\rm d}k_{\rm dif}}{{\rm d}\varphi} = \frac{k_{\rm dif}}{3(1-\varphi)}\left[1+2\left(1+\alpha_{\rm dif}+\frac{1}{3}\alpha_{\rm dif}^2\right)\right] \quad \text{(planar pores)} \tag{70b}$$

Self-consistent scheme. A spherical shape is chosen to represent the solid phase. Eq. (62) directly applies to the medium with tubular pores, while for planar pores it becomes:

$$(1-\varphi)\,\frac{3\left(3+3\alpha_{s,\rm sc}+\alpha_{s,\rm sc}^2\right)}{2R_s^2} \;-\; \varphi\, r_{\rm sc}\left[\frac{1}{3}+\frac{2}{3}\left(1+\alpha_{\rm p,sc}+\frac{1}{3}\alpha_{\rm p,sc}^2\right)\right] = 0 \tag{71}$$

where $\alpha_{i,\rm sc} = R_i\sqrt{r_{\rm sc}}$ and $R_s = 3R_p$ from (60).

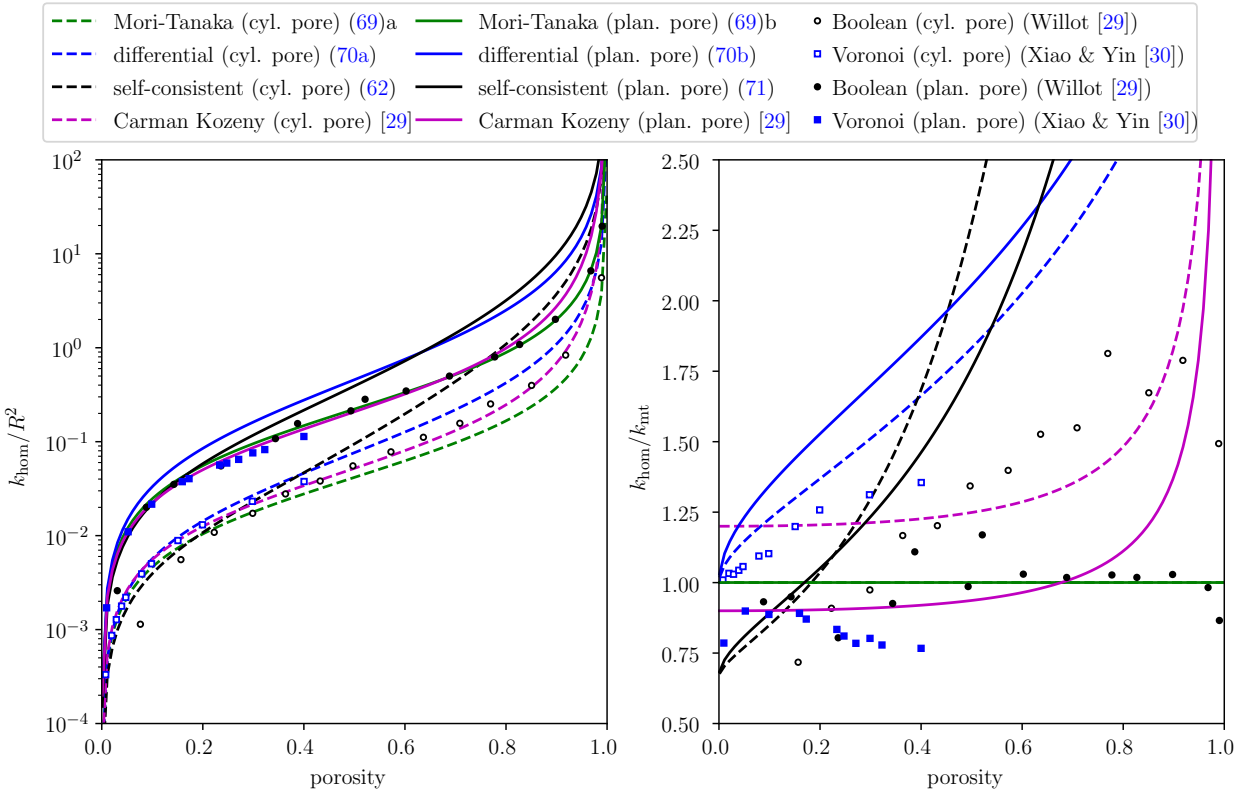

Figure 7: Permeability of a porous medium with cylindrical or planar pores of equal radius R or thickness $2R$, as a function of the porosity φ. Comparison to numerical simulations on Boolean models of elongated (fig. 4b) or flat cylinders (fig. 4c) [29] and tubular (resp. granular) media built from Voronoi diagrams eroded at edges (resp. faces) [30]. The specific surface area in the Carman Kozeny estimate is taken from the Boolean models [29].

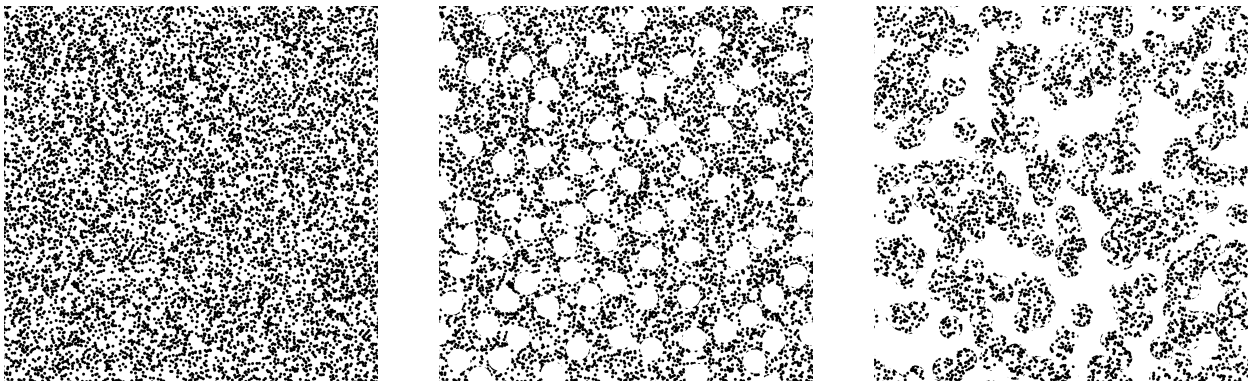

(a) Boolean disks

(b) double porosity with microporous matrix and disconnected mesopores

(c) double porosity with microporous grains

Figure 8: Some realizations of microstructures used in 2D FFT simulations (a) Boolean models of disks with porosity 65% (b) Double porosity medium with disconnected mesopores: meso-porosity 25%, micro-porosity 65%, total porosity 73.5%, size ratio of mesopores to micrograins 8 (c) Double porosity medium with microporous Boolean disks (meso-porosity 40%, micro-porosity 65%, total porosity 79%), size ratio of mesograins to micrograins 8

All estimates reproduce the overall trend of models as seen from figure 7, left. Rescaling the results by (69) provides more details: for planar pores, the best agreement with Boolean or eroded Voronoi models is obtained with the Mori-Tanaka scheme. For cylindrical pores, numerical models lie between the Mori-Tanaka and the differential scheme. The Carman Kozeny estimate (see [29] for details) is well suited, except at the highest permeabilities.

5.4. Double porosity materials

5.4.1. Simulations

Models. A series of simulations is carried out on model microstructures discretized on uniform grids using the algorithm based on the Stokes fluid Green function and Fast Fourier Transform described in [31]. Three types of microstructure models are investigated:

(a) a single porosity model of Boolean disks (figure 8a), which serves as a reference porous medium

(b) a double porosity model with mesopores created by carving out non overlapping disks in the medium of model (a) (figure 8b)

(c) a double porosity model with mesopores created by retaining the medium of model (a) only inside the disks of a Boolean model of larger disks, leaving the complementary space as mesopores (figure 8c)

For double porosity models (b) and (c), the total porosity is:

$$\varphi_{\text{tot}} = \varphi_{\text{meso}} + (1 - \varphi_{\text{meso}})\varphi_{\text{micro}} \tag{72}$$

where φ_{meso} is the volume fraction of meso-pores in the RVE and φ_{micro} is the intrinsic porosity of the micro-porous region, i.e. the volume of micro-pores divided by the sum of the volumes of micro-pores and micro-grains.

In model (a) the pores are connected provided the porosity lies above the percolation threshold of the Boolean model of disks, that is for porosities above $\varphi_c = 0.323661$ according to [102]. As the Representative Volume Element size for the permeability increases strongly near the percolation threshold [28, 31], simulations are carried out for porosities above 40%, up to 99%. In model (b) the mesoporosity is disconnected, meaning that the fluid must penetrate the micropores to join two mesopores. As a result, the mesoporosity is expected to have a moderate impact on the increase of the macroscopic permeability. In model (c), the connectivity of the mesopores depends on the position of the mesoporosity w.r.t. the percolation threshold of the Boolean model of disks. The permeability is thus expected to undergo a drastic increase as the

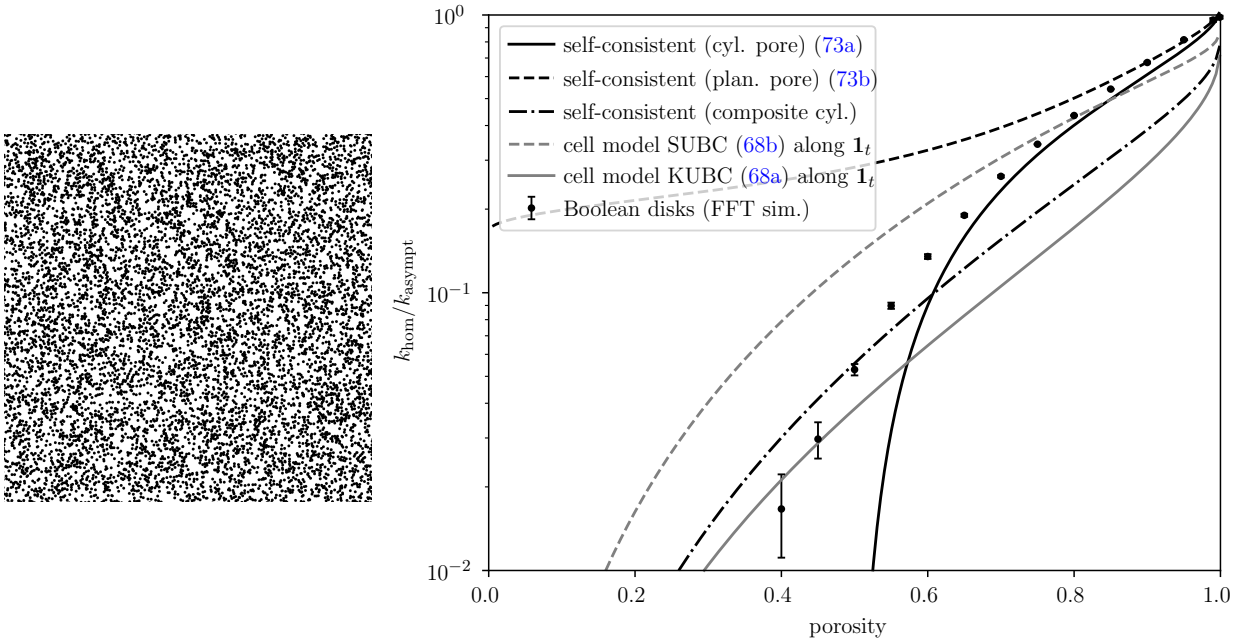

Figure 9: Permeability of the 2D Boolean model of disks (model (a)) with impermeable disks of equal radius R, scaled by $k_{\text{asympt}} = \frac{-\ln(1-\varphi)R^2}{8(1-\varphi)}$, as a function of the porosity φ.

mesoporosity exceeds φ_c. Simulations are carried out on realizations with target mesoporosity between 5% and 40% for model (b) and between 10% and 90% for model (c).

Note that unlike simulations in [103] where Darcy equations are assumed in the microporous domain and Stokes equations in the mesopores, present simulations are sufficiently refined so that the both the micropores and mesopores are discretized on the same large simulation, assuming Stokes equations in all types of pores, as in [82]. Hence, the present simulations are free of assumptions that would arise concerning the Darcy-Stokes interface. Obviously, such simulations are quite demanding to obtain both accurate and representative results, even in a two-dimensional setting.

Discretization errors and representativity of simulations. First, the accuracy is assessed by carrying out simulations on three nested discretization grids (512^2, 1024^2, 2048^2) for each random realization of the models. The computational time for a single simulation on the finest 2048^2 grid ranges from 60 seconds for the most porous samples to 300 seconds for the least porous samples, namely model (a) with $\varphi = 0.4$, on a standard office computer with CPU frequency 3.2GHz and parallelization on 8 threads. In the finest grid, the ratio of the disk diameter d to pixel size h is 16 (this is the diameter of the micro disks for models (b) and (c)). Plots of the computed permeability w.r.t. to h/d show linear trends which are fitted to extrapolate results to $h/d \to 0$. Further, for model (a) only, the effect of the discretization procedure is investigated by choosing three variants among the procedures described in [31], namely : the energy-consistent, rotated or forward-backward Green operators, together with force placement assumptions @center, @vertex or @face of the pixels respectively. The procedure energy-consistent@center (resp. rotated@vertex) yields decreasing (resp. increasing) computed permeability as h/d decreases and allows to bound the permeability, while the procedure forward-backward@face yields intermediate values for the lowest half of investigated porosities. Extrapolated values of the computed permeabilities using the three procedures have been used to display the error bars in figure 9: the accuracy is high for porosities above 50% but worsens as the porosity approaches the percolation threshold. For the porosity 65% selected for the background microporous material in models (b) and (c), the discretization error is negligible. With the addition of larger mesopores, the discretization error is further reduced. Hence, discretization errors are not reported on figures 10, model (b) and 11,

model (c).

Second, the representativity of simulations is addressed by two methods. At each porosity or mesoporosity, n realizations of the random microstructure model are performed ($n = 20$ for model (a), $n = 10$ for models (b) and (c)), and simulated on three grid sizes as stated above. The 95% confidence interval around the mean value is computed from the standard deviation D_k of the extrapolated permeabilities as $2D_k/\sqrt{n}$, the corresponding representativity error bars are displayed in the results of figures 10, model (b) and 11, model (c). For model (a), the methodology used in [31, section 4] to estimate the expected standard deviation from the integral range – which is a mesure of the volume of self-correlation of the velocity field – shows a good agreement with observed standard deviations from $n = 20$ realizations at each porosity. The relative representativity error $\epsilon_k^{RVE} = 2D_k/(\sqrt{n}k_{\rm hom})$ expected from a single realization (resp. from $n = 20$ simulations) is below 7.5% (resp. 1.7%) for all studied porosities in model (a) and 5.7% (resp 1.3%) for the selected porosity 65%. To reach $\epsilon_k^{RVE} = 5\%$ from a single simulation for the porosity 65%, the size L of the simulation box is estimated to about 145 times the disk diameter d according to the methodology used in [28, 31], which is much larger than for 3D simulations with the Boolean model of spheres [28]. We have used $L/d = 128$ in all simulations.

The permeability of model (a) at porosity $\varphi = 65\%$ is $k_{\rm micro}/R_{\rm micro}^2 = 0.072 \pm 0.001$. Accordingly for double porosity models (b) and (c), selected ratios $R_{\rm meso}/R_{\rm micro}$ of 2, 4, 8, 16 correspond to dimensionless parameter $\alpha = R_{\rm meso}/\sqrt{k_{\rm micro}}$ values equal to 7.4, 14.9, 29.7, 59.4 respectively at the mesoscopic scale.

5.4.2. Assessment of homogenization schemes

Model (a). The dilute, Mori-Tanaka and differential scheme which start from a clear fluid reference medium are discarded for the reasons discussed in sections 5.1 and 5.2. The self-consistent estimate (48) is built from cylindrical impermeable inhomogeneities (A.9b) of radius $R_s = R$ together with a cylindrical (A.9a) or planar (A.12a) Stokes inhomogeneity of radius R_p with $R_p = R_s$ for the cylindrical pore and $R_p = 2R_s$ for the planar pore from (60). The implicit equation for cylindrical (73a) or planar (73b) pores are, with $\alpha_{i,\rm sc} = R_i\sqrt{r_{\rm sc}}$:

$$(1-\varphi)\frac{\big(2+\alpha_{s,\rm sc}K_1^0(\alpha_{s,\rm sc})\big)}{\alpha_{s,\rm sc}K_1^0(\alpha_{s,\rm sc})} - \varphi\frac{8+\alpha_{p,\rm sc}^2+4\alpha_{p,\rm sc}K_1^0(\alpha_{p,\rm sc})}{16+\alpha_{p,\rm sc}^2+4\alpha_{p,\rm sc}K_1^0(\alpha_{p,\rm sc})} = 0 \quad \text{(disk pores)} \tag{73a}$$

$$(1-\varphi)\frac{2\big(2+\alpha_{s,\rm sc}K_1^0(\alpha_{s,\rm sc})\big)}{\alpha_{s,\rm sc}K_1^0(\alpha_{s,\rm sc})} - \frac{\varphi}{2}\big[1+\big(1+\alpha_{p,\rm sc}+\alpha_{p,\rm sc}^2/3\big)\big] = 0 \quad \text{(planar pores)} \tag{73b}$$

where a plane isotropy of the planar pores is assumed in (73b). The self-consistent estimate for a composite cylinder is derived by analogy with (63). It lies between the transverse components of cylindrical cell models (68), see figure 9. The trends of figure 5 for spherical grains are retrieved. Eqs. (73a) and (73b) are respectively below and above the simulation results for model (a). Eq. (73a) percolates at $\varphi = \frac{1}{2}$ but provides a reasonable agreement with simulation results for $\varphi \geq 60\%$.

Model (b). Let $\varphi_{\rm meso}$ denote the volume fraction of mesopores of radii $R_{\rm meso}$, $\boldsymbol{k}_0$ the permeability of the microporous phase, $\boldsymbol{r}_0$ its inverse and $\alpha_0 = R_{\rm meso}/\sqrt{k_0}$. From (A.9a), the Mori-Tanaka estimate (46) of the homogenized resistance is:

$$r_{\rm mt} = \frac{(1-\varphi_{\rm meso})r_0}{(1-\varphi_{\rm meso})+\varphi_{\rm meso}A_{1,0}} \text{ with } A_{1,0} = 2\frac{8+\alpha_0^2+4\alpha_0K_1^0(\alpha_0)}{16+\alpha_0^2+4\alpha_0K_1^0(\alpha_0)} \tag{74}$$

The differential estimate is started from the initial condition $r_{\rm dif}(\varphi_{\rm meso} = 0) = r_0$ and the differential equation:

$$\frac{{\rm d}r_{\rm dif}}{{\rm d}\varphi_{\rm meso}} = -\frac{2}{1-\varphi_{\rm meso}}\frac{8+\alpha_{\rm dif}^2+4\alpha_{\rm dif}K_1^0(\alpha_{\rm dif})}{16+\alpha_{\rm dif}^2+4\alpha_{\rm dif}K_1^0(\alpha_{\rm dif})} \quad \text{with} \quad \alpha_{\rm dif} = R_{\rm meso}r_{\rm dif} \tag{75}$$

Considering that the inhomogeneity size used to represent the RVE is a disk much larger than $\sqrt{k_0}$ and plane isotropy, the Maxwell estimate (53) written in terms of resistance requires the RVE resistance contribution

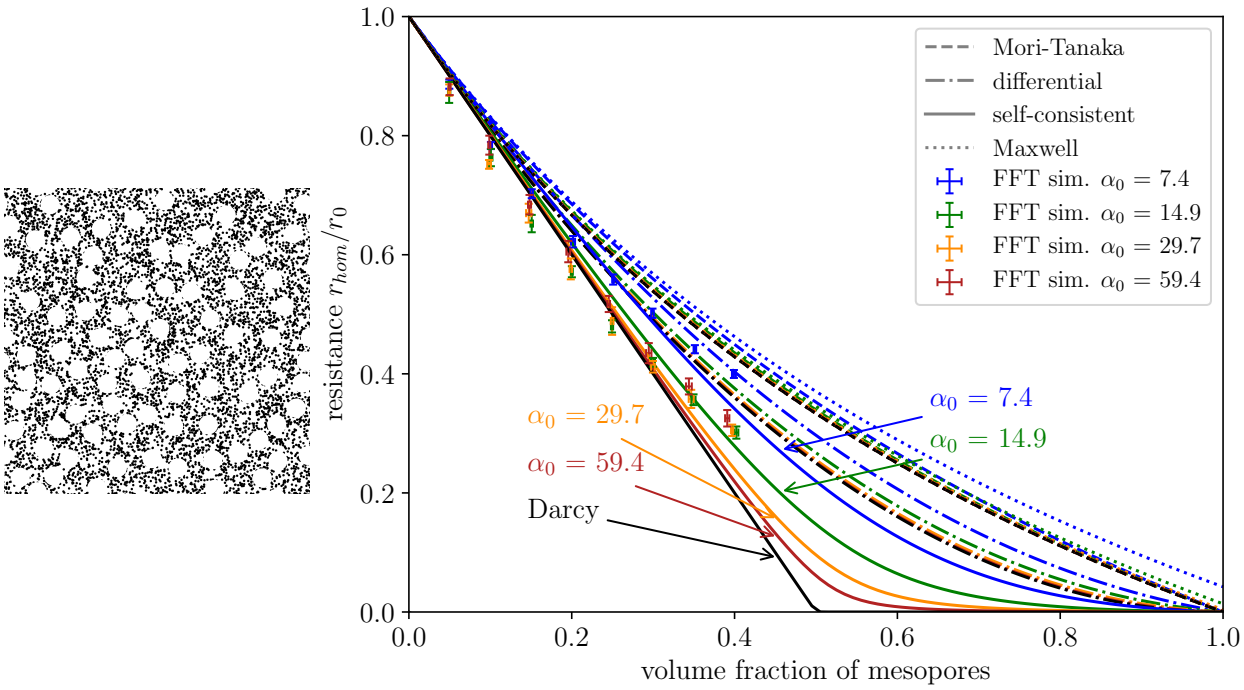

Figure 10: Permeability of the 2D double porosity material model (b) with microporosity $\varphi_{\text{micro}} = 65\%$, as a function of the mesoporosity φ_{meso}, for ratios of meso to micro disks of 2, 4, 8 and 16 (resp. $\alpha_0 = R_{\text{meso}}/\sqrt{k_{\text{micro}}} = 7.4$, 14.9, 29.7 and 59.4).

tensor $\boldsymbol{R}_{\text{RVE},0}$ in the Darcy limit whose in-plane components are $\left[(r_{\text{Max}} - r_0)^{-1} + (2r_0)^{-1}\right]^{-1}$. With $A_{1,0}$ defined as in (74), the Maxwell estimate to the resistance is:

$$r_{\text{Max}} = r_0 \left[1 - \left(\frac{1}{2} + \frac{1}{\varphi_{\text{meso}} A_{1,0}}\right)^{-1}\right] \tag{76}$$

Eq. (76) violates the Reuss bound (26) $r_{\text{app}} \leq \overline{r}^{\Omega} = (1 - \varphi_{\text{meso}})r_0$ at large mesoporosity. This confirms that, because size effects are inherent to Brinkman inhomogeneities, the transposition of Maxwell's scheme to Brinkman–Darcy upscaling is not appropriate.

The self-consistent estimate with cylindrical pores (A.9a) and microporous cylindrical grains (A.8) all of radii R_{meso} is solution to:

$$(1-\varphi_{\text{meso}})\frac{(r_0 - r_{\text{sc}})\alpha_{\text{sc}}\left\{\left[2(\alpha_0^2 - \alpha_{\text{sc}}^2) + \alpha_{\text{sc}}\alpha_0^2 K_1^0(\alpha_{\text{sc}})\right] I_0^1(\alpha_0) + \alpha_0\alpha_{\text{sc}}^2\right\}}{\left[2\alpha_{\text{sc}}(\alpha_0^2 - \alpha_{\text{sc}}^2) + \alpha_0^2(\alpha_0^2 + \alpha_{\text{sc}}^2)K_1^0(\alpha_{\text{sc}})\right] I_0^1(\alpha_0) + \alpha_{\text{sc}}\alpha_0(\alpha_{\text{sc}}^2 + \alpha_0^2)} - \varphi_{\text{meso}} r_{\text{sc}} \frac{8 + \alpha_{\text{sc}}^2 + 4\alpha_{\text{sc}}K_1^0(\alpha_{\text{sc}})}{16 + \alpha_{\text{sc}}^2 + 4\alpha_{\text{sc}}K_1^0(\alpha_{\text{sc}})} = 0 \tag{77}$$

with $\alpha_{\text{sc}} = R_{\text{meso}} r_{\text{sc}}$. Asymptotically as $R_{\text{meso}} \gg \sqrt{k_0}$, $r_{\text{sc}} \to r_0(1-2\varphi_{\text{meso}})$ if $\varphi_{\text{meso}} \leq \frac{1}{2}$ else 0, as in Darcy–Darcy upscaling with infinitely permeable cylindrical pores. The ordering of the Mori-Tanaka, differential and self-consistent schemes using Brinkman inhomogeneities is expected from the trends known in Darcy–Darcy (equivalent to conduction) upscaling. At low mesoporosity ($\varphi_{\text{meso}} \leq 25\%$), simulation results in figure 10 are slightly below the self-consistent estimate (77). At intermediate mesoporosity ($\varphi_{\text{meso}} \geq 30\%$), simulation results fall between the self-consistent (77) and differential (75) estimates, while the Mori-Tanaka one (74) overestimates the resistance.

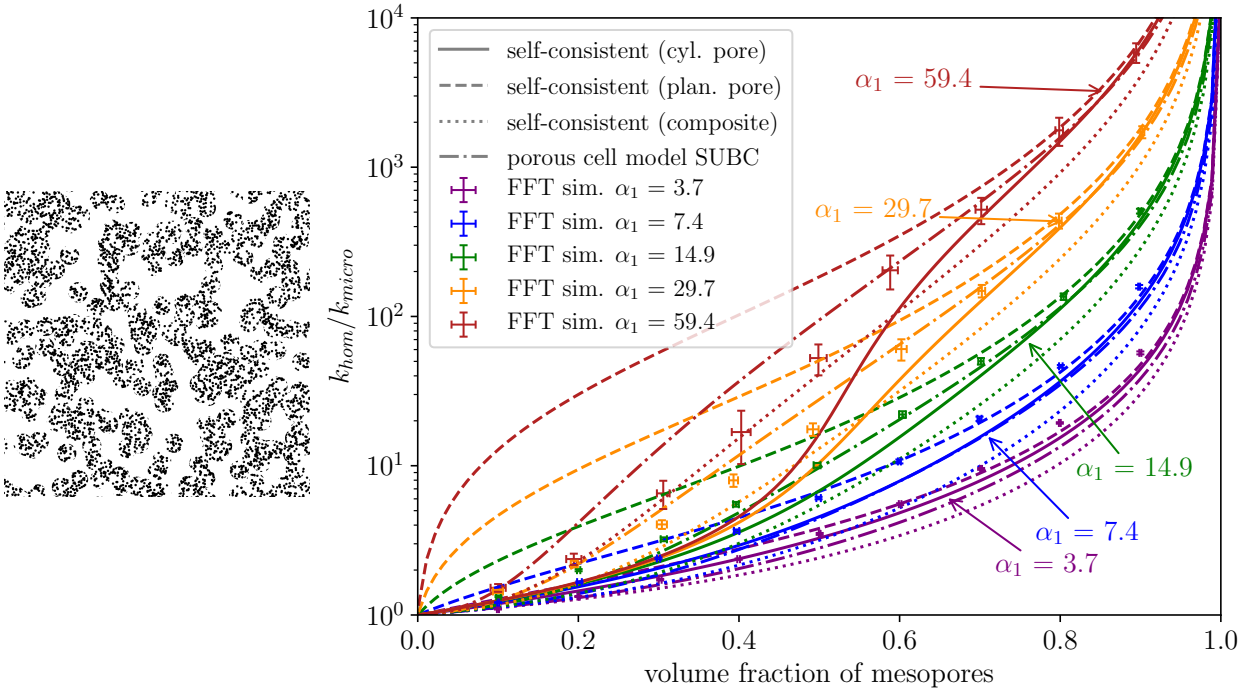

Figure 11: Permeability of the 2D double porosity material model (c) with microporosity $\varphi_{\text{micro}} = 65\%$, as a function of the mesoporosity φ_{meso}, for ratios of meso to micro disks of 1, 2, 4, 8 and 16 (resp. $\alpha_1 = R_{\text{meso}}/\sqrt{k_{\text{micro}}} = 3.7$, 7.4, 14.9, 29.7 and 59.4).

Model (c). The self-consistent estimate with microporous, disk-shaped grains is given by (77) for disk-shaped pores, and for planar pores with a plane isotropic distribution of orientations by:

$$(1-\varphi_{\text{meso}})\frac{(r_0-r_{\text{sc}})2\alpha_{\text{sc}}\left\{\left[2(\alpha_0^2-\alpha_{\text{sc}}^2)+\alpha_{\text{sc}}\alpha_0^2K_1^0(\alpha_{\text{sc}})\right]I_0^1(\alpha_0)+\alpha_0\alpha_{\text{sc}}^2\right\}}{\left[2\alpha_{\text{sc}}(\alpha_0^2-\alpha_{\text{sc}}^2)+\alpha_0^2(\alpha_0^2+\alpha_{\text{sc}}^2)K_1^0(\alpha_{\text{sc}})\right]I_0^1(\alpha_0)+\alpha_{\text{sc}}\alpha_0(\alpha_{\text{sc}}^2+\alpha_0^2)}-\frac{\varphi_{\text{meso}}}{2}r_{\text{sc}}\left[1+\left(1+\alpha_{p,\text{sc}}+\alpha_{p,\text{sc}}^2/3\right)\right]=0 \tag{78}$$

The self-consistent estimates (77) and (78) are compared in figure 11 to simulations results for model (c). The asymptotic trend as $\varphi_{\text{meso}} \to 1$ is well reproduced. The use of planar pores (78) (resp disk pores (77)) tends to overestimate (resp. underestimate) the simulation results, which is directly attributed to the over- or underestimation of the mesoporosity percolation thresholds, as for model (a).

The cell model with SUBC (generalized Happel model) and porous core surrounded by a fluid envelope with size ratio $\eta = \sqrt{1-\varphi_{\text{meso}}}$ gives a permeability for flow transverse to cylinder axis equal to (see e.g. [51]):

$$\begin{aligned} k_{\text{app,transverse}}^{\text{SUBC}} = R^2 \big\{ & 8\eta^4\alpha_1^3\ln\eta + 2\alpha_1^3 - (2\alpha_1^3+32\alpha_1)\eta^4 \\ & + \left[(12\alpha_1^2+\alpha_1^4+64)\eta^4 - \alpha_1^4 + 4\alpha_1^2 - (2\alpha_1^4+(2\alpha_1^4+16\alpha_1^2)\eta^4)\ln\eta\right] I_0^1(\alpha_1)\big\} \\ & / \, 8\left\{\left[(8+\alpha_1^2)\eta^4+\alpha_1^2\right] I_0^1(\alpha_1) - 4\eta^4\alpha_1\right\}\alpha_1^2\eta^2 \end{aligned} \tag{79}$$

The self-consistent estimate with the same composite inclusion, worked out from the general solution (A.7), is bounded by the cell model with SUBC (79) and KUBC (not detailed here, see e.g. [51]). For intermediate mesoporosity ($\varphi_{\text{meso}} \leq 0.6$) and larger grains ($\alpha_1 \geq 14.9$), schemes based on composite inclusions are in closer agreement with simulation results than (77), (78)) due to issues on the mesoporosity percolation threshold discussed above.

6. Conclusion

This work is a contribution towards the unification and generalization of existing schemes for permeability upscaling, as an extension of micromechanical estimates available for elasticity or conduction. The definition and study of generalized Brinkman inhomogeneities is demonstrated as an efficient way to formulate homogenization schemes suitable to Stokes to Darcy upscaling. The existing effective medium approximations with composite cells [52–57] or the iterated dilute approximation [66] naturally appear as special cases within the present formalism.

The Brinkman based homogenization schemes have been assessed against a panel of types of porous media, including granular and fibrous media, model materials with spanning flat or elongated pores as well as double porosity materials with either connected or disconnected mesoporosity. An important conclusion is that there is no universal homogenization scheme, but rather a diversity which is necessary to handle the variety of microstructure types. The Brinkman-based dilute, Mori-Tanaka, differential and self-consistent schemes behave similarly to their counterparts in elasticity or conduction upscaling, although permeability is a property extremely sensitive to microstructure characteristics. However, because of a size dependence inherent to Brinkman inhomogeneities, the transposed Maxwell's scheme appears ill-behaved and may violate Voigt-Reuss bounds. The self-consistent scheme delivers accurate results for higher porosity granular or fibrous materials, by far better than upper bounds build on more complex microstructure information such as three point volume and surface correlation functions [69]. Its potential to handle intermediate porosity must still be explored by resorting to more appropriate pore shapes, which have a direct impact on the percolation threshold.

Generalized inhomogeneities allow not only for simple shaped, uniform inclusion or cell based estimates as investigated here, but also in future and with additional computational effort, for more complex shapes akin to concave shaped pores [93–95] or any relevant morphological representative pattern [70, 104]. A first natural extension would be the spheroidal shape. The solution to Brinkman's flow inside spheroid slightly deformed from a sphere has been investigated in [105, 106] for a cell model. Solution to Brinkman equation for axial flow past an arbitrary spheroid is given in [96] but still missing for the transverse direction.

The homogenization schemes may mathematically handle anisotropic media as well as particle or pore size distributions, but their relevance has not been demonstrated herein. In particular, materials with continuous and spread size distributions raise fundamental issues related to scale separation. This aspect will be critical for real material applications.

Two fundamental points have been omitted from the current study: the effect of the effective fluid viscosity in Brinkman's equations and the impact of the jump momentum at the interface between two different porous media. The present framework will have to be extended as understanding will progress on these aspects.

The direct correspondence between the elasticity, conduction or Brinkman-based homogenization schemes opens the possibility for joint property upscaling in the spirit of [89], e.g. the simultaneous upscaling of stiffness, conduction and permeability of porous material from a shared microstructure description via inhomogeneities and homogenization schemes.

Funding. This research did not receive any specific grant from funding agencies in the public, commercial, or not-for-profit sectors.

Appendix A. Solutions to some Brinkman inhomogeneity problems

Appendix A.1. Spherical inhomogeneity

Brinkman equations admit separable solutions in the spherical coordinate system (r, θ, ϕ) when the permeability is isotropic, i.e. $\boldsymbol{k}_i = k_i \mathbf{1}$ in each medium i. The characteristic length $\ell_i = \sqrt{k_i}$ introduced. The velocity and pressure solutions to the inhomogeneity problem with remote velocity $\boldsymbol{V}_0 = V_0 \boldsymbol{e}_z$ with the

direction z corresponding to $\theta = 0$ are:

$$\begin{aligned} \boldsymbol{v} &= u(r)\cos(\theta)\boldsymbol{e}_r - (u(r) + \tfrac{1}{2} r\, u'(r))\sin(\theta)\boldsymbol{e}_\theta \\ u(r) &= c_{1,i} + c_{2,i} r^{-3} + c_{3,i}(\ell_i - r) r^{-3}\exp(r/\ell_i) + c_{4,i}(\ell_i + r) r^{-3}\exp(-r/\ell_i) \\ p &= \mu \ell_i^{-2}(-c_{1,i} r + \tfrac{1}{2} c_{2,i} r^{-2})\cos(\theta) \end{aligned} \tag{A.1}$$

For the medium $i = 1$ containing the origin, the coefficients must meet $c_{2,1} = 0$ and $c_{3,i} = c_{4,i}$ to avoid the diverging behavior as $r \to 0$. In the unbounded reference medium $i = 0$, the coefficients must meet $c_{3,0} = 0$ to avoid the diverging behavior as $r \to \infty$. The other coefficients are determined by solving the system of equations of continuity of the radial and tangential velocity and stress across the boundary between two phases.

Appendix A.1.1. Homogeneous spherical inhomogeneity

The average velocity localisation tensor (29) in a Brinkman sphere of radius R with isotropic permeability k_1 immersed in a reference Brinkman medium of permeability k_0 is:

$$\begin{aligned} \boldsymbol{A}_{1,0} &= 3\frac{\left(\alpha_0^3\alpha_1^2 - \beta\right)\tanh(\alpha_1) + \left(\alpha_0^2\alpha_1^2 + \beta\right)\alpha_1}{\left(\alpha_0^3\alpha_1^2 + 2\alpha_0\alpha_1^4 - \beta\right)\tanh(\alpha_1) + \left(\alpha_0^2\alpha_1^2 + 2\alpha_1^4 + \beta\right)\alpha_1}\mathbf{1} \\ \text{where} \quad \beta &= 3(\alpha_1^2 - \alpha_0^2)(1 + \alpha_0) \end{aligned} \tag{A.2}$$

with the dimensionless variables $\alpha_i = R/\sqrt{k_i}$ $(i = 0,\, 1)$. The following limiting cases of inhomogeneity types are useful:

$$\text{Stokes inhomogeneity} \qquad \lim_{k_1 \to \infty} \boldsymbol{A}_{1,0} = 3\frac{15 + 15\alpha_0 + 6\alpha_0^2 + \alpha_0^3}{45 + 45\alpha_0 + 6\alpha_0^2 + \alpha_0^3}\mathbf{1} \tag{A.3a}$$

$$\text{impervious inhomogeneity} \qquad \lim_{r_1 \to \infty} r_1 \boldsymbol{A}_{1,0} = \frac{3\left(3 + 3\alpha_0 + \alpha_0^2\right)}{2R^2}\mathbf{1} \tag{A.3b}$$

$$\text{Darcy inhomogeneity} \qquad \lim_{R \to \infty} \boldsymbol{A}_{1,0} = \frac{3k_1}{k_1 + 2k_0}\mathbf{1} \tag{A.3c}$$

Eq. (A.3b) times μV is the well known expression of Brinkman [60] for the drag force per unit volume experienced by a solid sphere in a Brinkman medium with remote velocity V. Eq. (A.3c) is the classical expression used in Darcy to Darcy homogenization. Eq. (A.3a) has not been used in previous Stokes to Darcy homogenization schemes [60, 66] but plays a key role in our version of the Stokes to Darcy self-consistent scheme or when dealing with double porosity materials (i.e. with porosity at several scales).

Appendix A.1.2. Composite spherical inhomogeneity

The average concentration tensors (29) of a composite spherical inhomogeneity ω_1 with impermeable core of radius R and Stokes shell of radius R/η with $\eta \in [0; 1]$ embedded in a Brinkman reference medium of isotropic permeability k_0 are:

$$\boldsymbol{A}_{1,0} = \frac{3(1-\eta)^2 N}{D}\mathbf{1} \qquad ; \qquad \boldsymbol{r}_{1,0} \cdot \boldsymbol{A}_{1,0} = \frac{18\eta^3 M}{R^2 D}\mathbf{1}$$

$$\text{where} \quad \begin{cases} N = 4\alpha_0^3 + (24 - \alpha_0)\alpha_0^2\eta + 3\alpha_0(20 + \alpha_0 - 2\alpha_0^2)\eta^2 \\ \qquad + (60 + 30\alpha_0 - 18\alpha_0^2 - \alpha_0^3)\eta^3 + (30 - 9\alpha_0^2 + 4\alpha_0^3)\eta^4 \\ M = 6\alpha_0^3 + 21\alpha_0^2\eta + 5\alpha_0(9 - \alpha_0^2)\eta^2 + 5(9 - \alpha_0^2)\eta^3 - \alpha_0^3\eta^5 - \alpha_0^2\eta^6 \\ D = 4\alpha_0^3 + 3\alpha_0^2(8 - 3\alpha_0)\eta + 45\alpha_0(4 - \alpha_0)\eta^2 \\ \qquad + 10(18 - 18\alpha_0 + \alpha_0^3)\eta^3 + 30\alpha_0^2\eta^4 - 9\alpha_0^3\eta^5 + \alpha_0^2(4\alpha_0 - 9)\eta^6 \end{cases} \tag{A.4}$$

with $\alpha_0 = R/\sqrt{k_0}$ and where (32) is used to compute the average leading to $\boldsymbol{r}_{1,0} \cdot \boldsymbol{A}_{1,0}$. The equivalent resistance of the composite sphere is defined according to (30) as:

$$\boldsymbol{r}_{1,0} = \frac{6\eta^3 M}{(1-\eta)^2 N R^2} \tag{A.5}$$

Solutions to composite n-layered spherical Brinkman inhomogeneities with finite permeability can be readily worked out from the general solution (A.1) in spherical geometry and appropriate continuity and boundary conditions, by a strategy similar to [107, 108]. General expressions are too lengthy to be reproduced herein.

Appendix A.2. Cylindrical inhomogeneity

The solution of the Brinkman cylindrical inhomogeneity of radius R and axis along the unit vector $\boldsymbol{n}$ with isotropic permeability $k_1 = \ell_1^2$ immersed in a reference Brinkman medium of permeability $k_0 = \ell_0^2$ is expressed in terms of the modified Bessel functions of order n of the first and second kind respectively denoted I_n and K_n. The cylindrical coordinate system (r, θ, z) is used with z along $\boldsymbol{n}$.

- *axial flow.* The solution to the inhomogeneity problem with remote body force $\boldsymbol{F}_0 = F_0 \boldsymbol{e}_z$ is:

$$p = F_0 z \quad ; \quad \boldsymbol{v} = (-F_0 \ell_i^2/\mu + c_{1,i} I_0(r/\ell_i) + c_{2,i} K_0(r/\ell_i))\boldsymbol{e}_z \tag{A.6}$$

  in each medium $i \in \{0, 1\}$. Coefficients $c_{1,0} = 0$ and $c_{2,1} = 0$ to avoid the diverging behavior as $r \to \infty$ and $r \to 0$ respectively, while $c_{2,0}$ and $c_{1,1}$ are determined from the continuity of the tangential velocity and stress across the boundary of the cylinder. The velocity concentration is expressed with regard to the remote velocity $V_0 = k_0 F_0/\mu$ far away from the cylinder.

- *transverse flow.* The solution to the inhomogeneity problem with remote velocity $\boldsymbol{V}_0 = V_0 \boldsymbol{e}_x$ with the direction x corresponding to $\theta = 0$ is

$$\begin{aligned} \boldsymbol{v} &= u(r)\cos(\theta)\boldsymbol{e}_r - (r\,u(r))'\sin(\theta)\boldsymbol{e}_\theta \\ u(r) &= c_{1,i} + c_{2,i} r^{-2} + c_{3,i} K_1(r/\ell_i) r^{-1} + c_{4,i} I_1(r/\ell_i) r^{-1} \\ p &= \mu \ell_i^{-2}(-c_{1,i} r + c_{2,i} r^{-1})\cos(\theta) \end{aligned} \tag{A.7}$$

  in each medium $i \in \{0, 1\}$. Coefficients $c_{4,0} = 0$ and $c_{2,1} = c_{3,1} = 0$ to avoid the diverging behavior as $r \to \infty$ and $r \to 0$ respectively, $c_{1,0} = V_0$ to meet the remote boundary condition while $c_{2,0}$ and $c_{1,1}, c_{4,1}$ are determined from the continuity of the radial and tangential velocity and stress across the boundary of the cylinder.

Note that rigorously, (A.6) (resp. (A.7)) is not the solution to a KUBC (resp. SUBC) problem, because the inhomogeneity is of infinite extension. The average of the velocity concentration tensor (29) over the cylindrical homogeneity is:

$$\begin{aligned} &\boldsymbol{A}_{1,0} = A_n \mathbf{1}_n + A_t \mathbf{1}_t \quad \text{with} \quad \mathbf{1}_n = \boldsymbol{n} \otimes \boldsymbol{n} \;;\; \mathbf{1}_t = (\mathbf{1} - \boldsymbol{n} \otimes \boldsymbol{n}) \\ &A_n = \frac{\alpha_0}{\alpha_1^3} \frac{\left[2(\alpha_1^2 - \alpha_0^2) + \alpha_0 \alpha_1^2 K_1^0(\alpha_0)\right] I_0^1(\alpha_1) + \alpha_1 \alpha_0^2 K_1(\alpha_0)}{\alpha_1 K_1^0(\alpha_0) I_0^1(\alpha_1) + \alpha_0} \\ &A_t = 2\alpha_0 \frac{\left[2(\alpha_1^2 - \alpha_0^2) + \alpha_0 \alpha_1^2 K_1^0(\alpha_0)\right] I_0^1(\alpha_1) + \alpha_1 \alpha_0^2}{(2\alpha_0(\alpha_1^2 - \alpha_0^2) + \alpha_1^2(\alpha_1^2 + \alpha_0^2) K_1^0(\alpha_0))\, I_0^1(\alpha_1) + \alpha_0 \alpha_1 (\alpha_0^2 + \alpha_1^2)} \end{aligned} \tag{A.8}$$

where $\alpha_i = R/\sqrt{k_i}$ $(i = 0,\ 1)$ are the dimensionless variables and $I_0^1(\alpha_1) = I_1(\alpha_1)/I_0(\alpha_1) \in [0; 1]$, $K_1^0(\alpha_0) = K_0(\alpha_0)/K_1(\alpha_0) \in [0; 1]$. The following limiting cases of inhomogeneity types are useful:

Stokes
$$\lim_{k_1 \to \infty} \boldsymbol{A}_{1,0} = \frac{8 + \alpha_0^2 + 4\alpha_0 K_1^0(\alpha_0)}{8} \mathbf{1}_n + 2\frac{8 + \alpha_0^2 + 4\alpha_0 K_1^0(\alpha_0)}{16 + \alpha_0^2 + 4\alpha_0 K_1^0(\alpha_0)} \mathbf{1}_t \tag{A.9a}$$

impervious
$$\lim_{r_1 \to \infty} r_1 \boldsymbol{A}_{1,0} = \frac{\alpha_0 \left(2 + \alpha_0 K_1^0(\alpha_0)\right)}{K_1^0(\alpha_0) R^2} (\mathbf{1}_n + 2\mathbf{1}_t) \tag{A.9b}$$

Darcy
$$\lim_{R \to \infty} \boldsymbol{A}_{1,0} = \frac{k_1}{k_0} \mathbf{1}_n + \frac{2k_1}{k_0 + k1} \mathbf{1}_t \tag{A.9c}$$

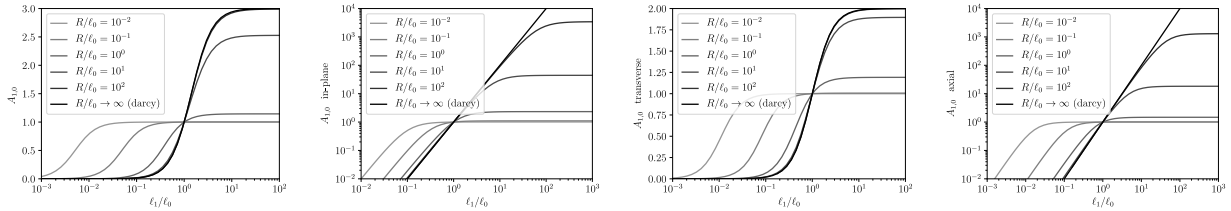

(a) spherical (b) planar, in plane flow (c) cylindrical, transverse flow (d) cylindrical, axial flow

Figure A.12: Average velocity concentration tensor (29) in a homogenenous Brinkman inhomogeneity of permeability $k_1 = \ell_1^2$ in a reference Brinkman medium of permeability $k_0 = \ell_0^2$.

as well as, when dealing with low permeabilities:

$$\begin{aligned} I_0^1(\alpha_1) &= \frac{I_1(\alpha_1)}{I_0(\alpha_1)} = 1 - \tfrac{1}{2}\alpha_1^{-1} - \tfrac{1}{8}\alpha_1^{-2} - \tfrac{1}{8}\alpha_1^{-3} - \tfrac{25}{128}\alpha_1^{-4} - \tfrac{13}{32}\alpha_1^{-5} + o\left(\alpha_1^{-5}\right) \quad \text{as } \alpha_1 \gg 1 \\ K_1^0(\alpha_0) &= \frac{K_0(\alpha_0)}{K_1(\alpha_0)} = 1 - \tfrac{1}{2}\alpha_0^{-1} + \tfrac{3}{8}\alpha_0^{-2} - \tfrac{3}{8}\alpha_0^{-3} + \tfrac{63}{128}\alpha_0^{-4} - \tfrac{27}{32}\alpha_0^{-5} + o\left(\alpha_0^{-5}\right) \quad \text{as } \alpha_0 \gg 1 \end{aligned} \tag{A.10}$$

Appendix A.3. Planar inhomogeneity

In the case where the inhomogeneity is the space comprised between the two planes $z = \pm R$ of unit normal $\boldsymbol{n}$, with isotropic permeability $k_1 = \ell_1^2$, immersed in a reference Brinkman medium of permeability $k_0 = \ell_0^2$, the solution to the inhomogeneity problem is obtained in Cartesian coordinate system (x, y, z):

- *flow perpendicular to the planes.* the solution to the inhomogeneity problem with remote velocity $\boldsymbol{V}_0 = V_0 \boldsymbol{e}_z$ is the uniform velocity $\boldsymbol{v} = V_0 \boldsymbol{e}_z$ so that the velocity concentration tensor component zz is 1.
- *flow parallel to the planes.* (say in direction x) the solution to the SUBC problem with remote drag force density $\boldsymbol{F}_0 = F_0 \boldsymbol{e}_x$ is $p = F_0 x$ and $\boldsymbol{v} = (-F_0 \ell_i^2/\mu + c_{1,i} \exp(z/\ell_i) + c_{2,i} \exp(-z/\ell_i))\boldsymbol{e}_x$ in the layer i of permeability $k_i = \ell_i^2$. Coefficient $c_{j,i}$ are matched to obtained continuity of the tangential velocity and stress across the planes. The velocity concentration is expressed with regard to the remote velocity $V_0 = -k_0 F_0/\mu$ far away from the planar inhomogeneity.

The average velocity concentration tensor (29) over the planar inhomogeneity is:

$$\boldsymbol{A}_{1,0} = \mathbf{1}_n + \frac{\left[\left(\alpha_1^2(1+\alpha_0) - \alpha_0^2\right)\tanh(\alpha_1) + \alpha_0^2\alpha_1\right]\alpha_0}{\alpha_1^3\left(\alpha_1 \tanh(\alpha_1) + \alpha_0\right)}\mathbf{1}_t \tag{A.11}$$

where $\alpha_i = R/\sqrt{k_i}$ $(i = 0,\ 1)$ are the dimensionless variables. The following limiting cases of inhomogeneity types are useful:

$$\text{Stokes inhomogeneity} \qquad \lim_{k_1 \to \infty} \boldsymbol{A}_{1,0} = \mathbf{1}_n + \left(1 + \alpha_0 + \frac{1}{3}\alpha_0^2\right)\mathbf{1}_t \tag{A.12a}$$

$$\text{impervious inhomogeneity} \qquad \lim_{r_1 \to \infty} r_1\left(\boldsymbol{A}_{1,0} - \mathbf{1}_n\right) = \frac{\alpha_0 + \alpha_0^2}{R^2}\mathbf{1}_t \tag{A.12b}$$

$$\text{Darcy inhomogeneity} \qquad \lim_{R \to \infty} \boldsymbol{A}_{1,0} = \mathbf{1}_n + \frac{k_1}{k_0}\mathbf{1}_t \tag{A.12c}$$

References

[1] A. Zaoui, Continuum Micromechanics: Survey, J. Eng. Mech. 128 (8) (2002) 808–816.
[2] L. Dormieux, D. Kondo, F.-J. Ulm, Microporomechanics, John Wiley & Sons, Ltd, Chichester, UK, 2006.
[3] V. Buryachenko, Micromechanics of Heterogenous Materials, Springer, Boston, MA, 2007.
[4] S. K. Kanaun, V. M. Levin, Self-Consistent Methods for Composites. Vol.1: Static Problems, Springer, Dordrecht, 2008.
[5] M. Kachanov, I. Sevostianov, Micromechanics of Materials, with Applications, Springer International Publishing, 2018.
[6] J. D. Eshelby, The determination of the elastic field of an ellipsoidal inclusion, and related problems, Proceedings of the Royal Society of London. Series A. Mathematical and Physical Sciences 241 (1226) (1957) 376–396.
[7] J. D. Eshelby, The elastic field outside an ellipsoidal inclusion, Proceedings of the Royal Society of London. Series A. Mathematical and Physical Sciences 252 (1271) (1959) 561–569.
[8] T. Mori, K. Tanaka, Average stress in matrix and average elastic energy of materials with misfitting inclusions, Acta Metallurgica 21 (1973) 571–574.
[9] Y. Benveniste, On the Mori-Tanaka method for cracked solids, Mech. Res. Comm. 13 (4) (1986) 193–201.
[10] R. Roscoe, The viscosity of suspensions of rigid spheres, British Journal of Applied Physics 3 (8) (1952) 267–269.
[11] H. C. Brinkman, The Viscosity of Concentrated Suspensions and Solutions, The Journal of Chemical Physics 20 (4) (1952) 571–571.
[12] R. Roscoe, Isotropic composites with elastic or viscoelastic phases: General bounds for the moduli and solutions for special geometries, Rheologica Acta 12 (3) (1973) 404–411.
[13] S. Boucher, Modules effectifs de matériaux composites quasi homogènes et quasi isotropes, constitués d'une matrice élastique et d'inclusions élastiques. II. Cas des concentrations finies en inclusions, Revue M. Mec. 22 (1) (1976) 31–36.
[14] R. McLaughlin, A study of the differential scheme for composite materials, International Journal of Engineering Science 15 (4) (1977) 237–244.
[15] A. Norris, A differential scheme for the effective moduli of composites, Mechanics of Materials 4 (1) (1985) 1–16.
[16] J. C. Maxwell, A treatise on electricity and magnetism., Clarendon Press, Oxford, 1873.
[17] I. Sevostianov, A. Giraud, Generalization of Maxwell homogenization scheme for elastic material containing inhomogeneities of diverse shape, International Journal of Engineering Science 64 (2013) 23–36.
[18] D. A. G. Bruggeman, Berechnung verschiedener physikalischer Konstanten von heterogenen Substanzen. I. Dielektrizitätskonstanten und Leitfähigkeiten der Mischkörper aus isotropen Substanzen, Annalen der Physik 416 (7) (1935) 636–664.
[19] A. V. Hershey, The elasticity of an isotropic aggregate of anisotropic cubic crystals, J. Appl. Mech. 21 (1954) 236–240.
[20] E. Kröner, Berechnung der elastischen Konstanten des Vielkristalls aus den Konstanten des Einkristalls, Zeitschrift für Physik 151 (4) (1958) 504–518.
[21] R. Hill, A self-consistent mechanics of composite materials, Journal of the Mechanics and Physics of Solids 13 (4) (1965) 213–222.
[22] B. Budiansky, On the elastic moduli of some heterogeneous materials, Journal of the Mechanics and Physics of Solids 13 (4) (1965) 223–227.
[23] S. Prager, Viscous Flow through Porous Media, Phys. Fluids 4 (1961) 1477–1482.
[24] G. Matheron, Élements pour une théorie des milieux poreux, Paris, Masson, 1967.
[25] H. Ene, E. Sanchez-Palencia, Equations et phénomènes de surface pour l'écoulement dans un modèle de milieu poreux, Journal de Mécanique (1975) 73–108.
[26] J.-L. Auriault, E. Sanchez-Palencia, Etude du comportement macroscopique d'un milieu poreux saturé déformable, Journal de Mécanique 16 (1977) 575–603.
[27] S. Whitaker, Flow in porous media I: A theoretical derivation of Darcy's law, Transport in Porous Media 1 (1) (1986) 3–25.
[28] B. Abdallah, F. Willot, D. Jeulin, Stokes flow through a Boolean model of spheres: Representative volume element, Transport in Porous Media 109 (3) (2015) 711–726.
[29] F. Willot, B. Abdallah, D. Jeulin, The Permeability of Boolean Sets of Cylinders, Oil & Gas Science and Technology - Revue d'IFP Energies nouvelles 71 (4).
[30] F. Xiao, X. Yin, Geometry models of porous media based on Voronoi tessellations and their porosity-permeability relations, Computers & Mathematics with Applications 72 (2) (2016) 328 – 348, ISSN 0898-1221, the Proceedings of ICMMES 2014.
[31] F. Bignonnet, Efficient FFT-based upscaling of the permeability of porous media discretized on uniform grids with estimation of RVE size, Computer Methods in Applied Mechanics and Engineering 369 (2020) 113237.
[32] Q. Xiong, T. G. Baychev, A. P. Jivkov, Review of pore network modelling of porous media: Experimental characterisations, network constructions and applications to reactive transport, Journal of Contaminant Hydrology 192 (2016) 101–117.
[33] P. C. Carman, Fluid flow through granular beds, Trans.-Inst. Chem. Eng. 15 (1937) 150–166.
[34] L. Dormieux, E. Lemarchand, Homogenization Approach of Advection and Diffusion in Cracked Porous Material, Journal of Engineering Mechanics 127 (2001) 1267–1274.
[35] L. Dormieux, D. Kondo, Approche micromécanique du couplage perméabilité-endommagement, Comptes Rendus Mécanique 332 (2) (2004) 135–140, ISSN 1631-0721.
[36] J.-F. Barthélémy, Effective permeability of media with a dense network of long and micro fractures, Transp. Porous Media 76 (2009) 153–178.

[37] L. Dormieux, L. Jeannin, N. Gland, Homogenized models of stress-sensitive reservoir rocks, International Journal of Engineering Science 49 (5) (2011) 386–396.
[38] L. Jeannin, F. Bignonnet, F. Agostini, Y. Wang, Stress effects on the relative permeabilities of tight sandstones, Comptes Rendus Geoscience 350 (3) (2018) 110–118.
[39] J. J. Timothy, G. Meschke, Cascade Lattice Micromechanics Model for the Effective Permeability of Materials with Microcracks, Journal of Nanomechanics and Micromechanics 6 (4) (2016) 04016009.
[40] E. Cunningham, On the velocity of steady fall of spherical particles through fluid medium, Proceedings of the Royal Society of London. Series A, Containing Papers of a Mathematical and Physical Character 83 (563) (1910) 357–365.
[41] J. Happel, Viscous flow in multiparticle systems: slow motion of fluids relative to beds of spherical particles., AIChE J. 4 (1958) 197–201.
[42] J. Happel, Viscous Flow Relative to Arrays of Cylinders, AIChE J. 5 (1959) 174–177.
[43] G. Neale, N. Epstein, W. Nader, Creeping flow relative to permeable spheres, Chemical Engineering Science 28 (10) (1973) 1865–1874.
[44] A. L. Berdichewsky, Z. Cai, Preform permeability predictions by self-consistent method and finite element simulation, Polymer composites 14 (2) (1993) 132–143.
[45] C. Boutin, Study of permeability by periodic and self-consistent homogenisation, European Journal of Mechanics A/Solids 19 (2000) 603–632.
[46] S. Kuwabara, The Forces experienced by Randomly Distributed Parallel Circular Cylinders or Spheres in a Viscous Flow at Small Reynolds Numbers, J. Phys. Soc. Jpn. 14 (1959) 527–532.
[47] G. Dassios, M. Hadjinicolaou, F. Coutelieris, A. Payatakes, Stokes flow in spheroidal particle-in-cell models with Happel and Kuwabara boundary conditions, Int. J. Engng Sci. 33 (1995) 1465–1490.
[48] R. H. Davis, H. A. Stone, Flow through beds of porous particles, Chemical Engineering Science 48 (23) (1993) 3993–4005.
[49] S. I. Vasin, A. N. Filippov, Permeability of complex porous media, Colloid Journal 71 (1) (2009) 31.
[50] J. Prakash, G. P. Raja Sekhar, K. Mirela, Stokes flow of an assemblage of porous particles: stress jump condition, Zeitschrift für angewandte Mathematik und Physik 62 (6) (2011) 1027–1046.
[51] S. Deo, A. Filippov, A. Tiwari, S. Vasin, V. Starov, Hydrodynamic permeability of aggregates of porous particles with an impermeable core, Advances in Colloid and Interface Science 164 (2001) 21–37.
[52] H. C. Brinkman, On the permeability of media consisting of closely packed porous particles, Appl. Sci. Res. A1 (1947) 81.
[53] G. H. Neale, W. K. Nader, Prediction of transport processes within porous media: Creeping flow relative to a fixed swarm of spherical particles, AIChE Journal 20 (3) (1974) 530–538.
[54] Y. Li, C.-W. Park, Effective medium approximation and deposition of colloidal particles in fibrous and granular media, Advances in Colloid and Interface Science 87 (1) (2000) 1–74.
[55] B. Albusairi, J. T. Hsu, Flow through beds of perfusive particles: effective medium model for velocity prediction within the perfusive media, Chemical Engineering Journal 100 (2004) 79–84.
[56] G. Raja Sekhar, Effective medium model for flow through beds of porous cylindrical fibres, Applicable Analysis 89 (6) (2010) 833–848.
[57] J. Prakash, G. P. Raja Sekhar, Overall bed permeability for flow through beds of permeable porous particles using the effective medium model-stress jump condition, Chemical Engineering Communications 198 (1) (2010) 85–101.
[58] J. Ochoa-Tapia, S. Whitaker, Momentum transfer at the boundary between a porous medium and a homogeneous fluid - Theoretical development, Int. J. Heat Mass Transf. 38 (1995) 2635–2646.
[59] J. Ochoa-Tapia, S. Whitaker, Momentum transfer at the boundary between a porous medium and a homogeneous fluid - Comparison with experiment, Int. J. Heat Mass Transf. 38 (1995) 2647–2655.
[60] H. C. Brinkman, A calculation of the viscous force exerted by a flowing fluid on a dense swarm of particles, Appl. Sci. Res. A1 (1947) 27.
[61] J.-L. Auriault, C. Geindreau, C. Boutin, Filtration Law in Porous Media with Poor Separation of Scales, Transport in Porous Media 60 (1) (2005) 89–108.
[62] E. Rohan, J. Turjanicova, V. Lukes, A Darcy-Brinkman model of flow in double porous media – Two-level homogenization and computational modelling, Computers & Structures 207 (2018) 95–110, ISSN 0045-7949, cIVIL-COMP 2017.
[63] I. Howells, Drag due to the motion of a Newtonian fluid through a sparse random array of small fixed rigid objects, J. Fluid Mech. 64 (3) (1974) 449–476.
[64] E. J. Hinch, An averaged-equation approach to particle interactions in a fluid suspension, J. Fluid Mech. 83 (4) (1977) 695–720.
[65] S. Kim, W. B. Russel, Modelling of porous media by renormalization of the Stokes equations, Journal of Fluid Mechanics 154 (1985) 269–286.
[66] D. Wilkinson, Modified drag theory of permeability, The Physics of Fluids 28 (4) (1985) 1015–1022.
[67] D. L. Brown, Y. Efendiev, G. Li, V. Savatorova, Homogenization of High-Contrast Brinkman Flows, Multiscale Modeling & Simulation 13 (2) (2015) 472–490.
[68] J. Rubinstein, S. Torquato, Flow in random porous media: mathematical formulation, variational principles, and rigorous bounds, J. Fluid Mech. 206 (1989) 25–46.
[69] F. Bignonnet, Upper Bounds on the Permeability of Random Porous Media, Transport in Porous Media 122 (1) (2018) 57–76, ISSN 1573-1634.
[70] M. Bornert, A generalized pattern-based self-consistent scheme, Computational Materials Science 5 (1) (1996) 17–31, computational Modelling of the Mechanical Behaviour of Materials.
[71] S. Childress, Viscous flow past a random array of spheres, J. Chem. Phys. 56 (6) (1972) 2527–2539.

[72] K. F. Freed, M. Muthukumar, On the Stokes problem for a suspension of spheres at finite concentrations, The Journal of Chemical Physics 68 (5) (1978) 2088–2096.
[73] T. Lévy, Fluid flow through an array of fixed particles, Int. J. Eng. Sci. 21 (1) (1983) 1983.
[74] G. Allaire, Homogenization of the Navier-Stokes equations with a slip boundary condition, Communications on Pure and Applied Mathematics 44 (6) (1991) 605–641.
[75] M. Quintard, S. Whitaker, Transport in ordered and disordered porous media II: Generalized volume averaging, Transport in Porous Media 14 (2) (1994) 179–206.
[76] J.-L. Auriault, On the Domain of Validity of Brinkman's Equation, Transport in Porous Media 79 (2) (2009) 215–223.
[77] F. Feppon, High Order Homogenization of the Stokes System in a Periodic Porous Medium, SIAM Journal on Mathematical Analysis 53 (3) (2021) 2890–2924.
[78] B. Goyeau, T. Benihaddadene, D. Gobin, M. Quintard, Averaged Momentum Equation for Flow Through a Nonhomogenenous Porous Structure, Transport in Porous Media 28 (1997) 19–50.
[79] M. Muthukumar, K. F. Freed, On the Stokes problem for a suspension of spheres at nonzero concentrations. II. Calculations for effective medium theory, The Journal of Chemical Physics 70 (12) (1979) 5875–5887.
[80] J. Koplik, H. Levine, A. Zee, Viscosity renormalization in the Brinkman equation, The Physics of Fluids 26 (10) (1983) 2864–2870.
[81] W.-P. Breugem, The effective viscosity of a channel-type porous medium, Physics of Fluids 19 (10) (2007) 103104.
[82] S. Zaripov, R. Mardanov, V. Sharafutdinov, Determination of Brinkman Model Parameters Using Stokes Flow Model., Transp Porous Med 130 (2019) 529–557.
[83] G. S. Beavers, D. D. Joseph, Boundary conditions at a naturally permeable wall, Journal of Fluid Mechanics 30 (1) (1967) 197–207.
[84] P. G. Saffman, On the Boundary Condition at the Surface of a Porous Medium, Studies in Applied Mathematics 50 (2) (1971) 93–101.
[85] Y. Sudhakar, U. Lacis, S. Pasche, B. S., Higher-Order Homogenized Boundary Conditions for Flows Over Rough and Porous Surfaces, Transp Porous Med 136 (2021) 1–42.
[86] A. G. Kvashnin, Cell model of suspension of spherical particles, Fluid Dynamics 14 (1979) 598–602.
[87] I. Sevostianov, M. Kachanov, Explicit cross-property correlations for anisotropic two-phase composite materials, Journal of the Mechanics and Physics of Solids 50 (2) (2002) 253–282.
[88] M. Kachanov, I. Sevostianov, On quantitative characterization of microstructures and effective properties, International Journal of Solids and Structures 42 (2) (2005) 309–336, micromechanics of Materials.
[89] M. Achour, F. Bignonnet, J.-F. Barthélémy, E. Rozière, O. Amiri, Multi-scale modeling of the chloride diffusivity and the elasticity of Portland cement paste, Construction and Building Materials 234 (2020) 117124.
[90] J. Y. Li, On micromechanics approximation for the effective thermoelastic moduli of multi-phase composite materials, Mechanics of Materials 31 (1999) 149–159.
[91] A. J. C. Ladd, Hydrodynamic transport coefficients of random dispersions of hard spheres, The Journal of Chemical Physics 93 (5) (1990) 3484–3494.
[92] L. Rong, K. Dong, A. Yu, Lattice-Boltzmann simulation of fluid flow through packed beds of uniform spheres: Effect of porosity, Chemical Engineering Science 99 (2013) 44 – 58, ISSN 0009-2509.
[93] F. Chen, I. Sevostianov, A. Giraud, D. Grgic, Evaluation of the effective elastic and conductive properties of a material containing concave pores, International Journal of Engineering Science 97 (2015) 60–68.
[94] A. Giraud, D. Grgic, I. Sevostianov, Effective elastic properties and thermal conductivity of isotropic rocks containing concave pores. Application to oolitic limestones, European Journal of Environmental and Civil Engineering (2020) 1–24.
[95] A. Markov, A. Trofimov, I. Sevostianov, A unified methodology for calculation of compliance and stiffness contribution tensors of inhomogeneities of arbitrary 2D and 3D shapes embedded in isotropic matrix – open access software., International Journal of Engineering Science 157 (2020) 103390.
[96] T. Zlatanovski, Axisymmetric creeping flow past a porous prolate spheroidal particle using the Brinkman model, The Quarterly Journal of Mechanics and Applied Mathematics 52 (1) (1999) 111–126.
[97] P. G. Saffman, On the Settling Speed of Free and Fixed Suspensions, Studies in Applied Mathematics 52 (2) (1973) 115–127.
[98] G. W. Jackson, D. F. James, The permeability of fibrous porous media, The Canadian Journal of Chemical Engineering 64 (1986) 364–374.
[99] C. N. Davies, The Separation of Airborne Dust and Particles, Proceedings of the Institution of Mechanical Engineers 167 (1b) (1953) 185–213.
[100] G. Neale, J. H. Masliyah, Flow perpendicular to mats of randomly arranged cylindrical fibers (importance of cell models), AIChE Journal 21 (4) (1975) 805–807.
[101] L. Spielman, S. Goren, Model for predicting pressure drop and filtration efficiency in fibrous media, Environmental Science & Technology 2 (1968) 279–287.
[102] J. Quintanilla, S. Torquato, R. M. Ziff, Efficient measurement of the percolation threshold for fully penetrable discs, Journal of Physics A: Mathematical and General 33 (42) (2000) L399–L407.
[103] S. Mezhoud, V. Monchiet, M. Bornert, D. Grande, Computation of macroscopic permeability of doubly porous media with FFT based numerical homogenization method, European Journal of Mechanics - B/Fluids 83 (2020) 141–155, ISSN 0997-7546.
[104] M. Bornert, C. Stolz, A. Zaoui, Morphologically representative pattern-based bounding in elasticity, Journal of The Mechanics and Physics of Solids 44 (1996) 307–331.
[105] E. I. Saad, Translation and rotation of a porous spheroid in a spheroidal container, Canadian Journal of Physics 88 (9)

(2010) 689–700.
[106] P. K. Yadav, S. Deo, M. K. Yadav, A. Filippov, On hydrodynamic permeability of a membrane built up by porous deformed spheroidal particles, Colloid Journal 75 (5) (2013) 611–622.
[107] E. Hervé, A. Zaoui, n-layered inclusion-based micromechanical modelling, Int. J. Engng. Sci. 31 (1993) 1–10.
[108] J.-F. Barthélémy, F. Bignonnet, The Eshelby problem of the confocal N-layer spheroid with imperfect interfaces and the notion of equivalent particle in thermal conduction, International Journal of Engineering Science 150 (2020) 103274.